Hf isotope systematics of seamounts near the East Pacific Rise (EPR) and geodynamic implications

Yu Zhang [a], Fanxue Meng [b, c]*, Yaoling Niu [b,d,e,]*

[a] School of Earth Sciences, Lanzhou University, Lanzhou 730000, China

[b] Institute of Oceanology, Chinese Academy of Sciences, Qingdao 266071, China

[c] College of Earth Science and Engineering, Shandong University of Science and Technology, Qingdao 266590, China

[d] Department of Earth Sciences, Durham University, Durham, DH1 3LE, UK

[e] School of Earth Sciences and Resources, China University of Geosciences, Beijing 100083, China

* Corresponding Authors: Dr. Fanxue Meng (mfx1117@163.com; mengfanxue@qdio.ac.cn)

Tel: +86 (532) 82898035

Professor Yaoling Niu (yaoling.niu@foxmail.com)

May 20, 2016 version

Abstract

We report new Hf isotopic data for basaltic glasses from seamounts flanking the East Pacific Rise (EPR) between 5° and 15°N that have been previously analyzed for Sr-Nd-Pb isotopes as well as major and trace elements. The Hf isotopic data offer new perspectives on the petrogenesis of these samples in a broader context on mantle dynamics. The Hf isotope compositions show significant correlations with Sr-Nd-Pb isotopes and with both abundances and ratios of incompatible elements. The seamount lavas are thus best interpreted as products of melting-induced mixing in a two-component mantle.

The range in composition of EPR seamount lavas cannot be generated by simple mixing of melt and melting of variably heterogeneous mantle in which enriched and depleted materials contribute equally to melting (source mixing). Instead, the trace element and isotope compositions of seamount lavas can be reproduced by melting models in which more enriched, fertile mantle component are preferentially melted during mantle upwelling. At progressively lower degrees of melting, erupted lavas are thus more enriched in incompatible trace elements, have higher $^{87}Sr/^{86}Sr$, $^{208}Pb/^{204}Pb$ ratios and lower $^{143}Nd/^{144}Nd$, $^{176}Hf/^{177}Hf$ ratios. The "EM1" and "pyroxenite" endmember might be the suitable enriched component.

The Hf-Nd isotopic variations on global scale might result from the variations in amounts of residual continental lithospheric mantle that detached into upper mantle during continental rifting. The significant correlations of Rb/Sr vs $^{87}Sr/^{86}Sr$, Sm/Nd vs $^{143}Nd/^{144}Nd$ and Lu/Hf vs $^{176}Hf/^{177}Hf$ give pseudochron ages of 182±33 Ma, 276±50 Ma and 387±93 Ma, respectively. These different "ages" have no significance, but result from melting-induced mixing with the pseudochron slopes controlled by the compositions of enriched

component and depleted end-member.

Keywords: East Pacific Rise; seamounts; melting-induced mixing; Hf isotopes; Hf-Nd correlation.

1. Introduction

Isotopic studies of oceanic basalts provide constraints on models of Earth's chemical differentiation and convection processes. One of the major advances in the solid Earth science over the past 50 years is the recognition of mantle compositional heterogeneity and the identification of several isotopically distinct mantle end-members through these isotopic studies (e.g., Gast et al., 1964; White, 1985; Zinder and Hart, 1986). Numerous geochemical studies of MORB (e.g. Allègre and Turcotte, 1986; Arevalo and McDonough, 2010; Donnelly et al., 2004; Hirschmann and Stolper, 1996; Niu et al., 1999; Phipps Morgan and Morgan, 1999; Schilling et al., 1983; Zindler and Hart, 1986; Haase et al., 2011; Brandl et al., 2012) have shown that even in the absence of nearby hotspots, the upper mantle is chemically and isotopically heterogeneous. The origin of these heterogeneities is debated, but they are likely results from recycled material (Donnelly et al., 2004; Niu and O'Hara, 2003; Pilet et al., 2005; White and Hofmann, 1982). The Nd and Hf isotope ratios (i.e., $^{143}Nd/^{144}Nd$ and $^{176}Hf/^{177}Hf$) are shown to be well correlated in ocean island basalts (OIB) due to the similar behavior during mantle melting the parent-daughter (P/D) pairs (i.e., $D_{Sm} > D_{Nd}$ and $D_{Lu} > D_{Hf}$) (Blichert-Toft, 2001; Patchett and Tatsumoto, 1980; Salters and Hart, 1991; Vervoort et al., 1996). In contrast to OIB, mid-ocean ridge basalts (MORB) on a global scale have large variations in Hf isotopic composition at a

given Nd isotopic composition (e.g., Blichert-Toft et al., 2005; Debaille et al., 2006; Johnson and Beard, 1993; Patchett, 1983; Patchett and Tastumoto, 1980; Salters and Hart, 1991; Salters and White, 1998; Salters and Zindler, 1995). A more recent study, however, shows that Hf and Nd isotopes in MORB are in fact well correlated on some ridge segment scales (Salters et al., 2011). This is an important observation that points to large regional scale differences in mantle sources and source histories.

To help address issues on MORB genesis and the variable MORB Hf-Nd isotopic correlations at different ridges (Salters et al., 2011), we study Hf isotope compositions of near-ridge seamounts flanking the East Pacific Rise (EPR) (see Fig. 1 and Fig. A1). We choose these seamount lavas because (1) they have already been well-characterized for major elements, trace elements, and Sr-Nd-Pb isotope compositions (Niu and Batiza, 1997; Niu et al, 2002); (2) they represent an integral part of EPR ridge magmatism as they were derived from the same upper mantle source of EPR axial MORB; (3) they have avoided melt homogenization during melt aggregation in the mantle and in the long-lived axial magma chambers, and thus more faithfully record the nature of the MORB mantle source beneath the EPR than axial lavas; and importantly, (4) they display a large compositional spectrum that encompasses much of the global MORB compositional variability from ridges unaffected by mantle plumes/hotspots, and can thus help answer first-order questions on MORB mantle sources and processes, especially beneath the fast-spreading EPR.

2. Samples and analytical methods

The samples were dredged during the 1988 Raitt 02 expedition aboard R/V Thomas

93 Washington (Batiza and Niu, 1992; Batiza et al., 1990). All the samples studied are basalt
94 glasses. They were collected from near-ridge seamounts within the 1 Ma isochron (< ~ 60
95 km) of the EPR axis between 5° and 15°N on both the Pacific and Cocos Plates (Fig. 1).
96 These 36 samples have been studied for major and trace elements (Batiza and Niu, 1992;
97 Batiza et al., 1990; Niu and Batiza, 1997) and Sr-Nd-Pb isotopes (all samples were
98 analyzed for Sr isotope, 28 of them were analyzed for Nd isotope and 34 of them were
99 analyzed for Pb isotope, see Niu et al., 2002).

100 All the samples were carefully hand-picked under a binocular microscope before they
101 were leached at room temperature in 10% H_2O_2 for a few minutes to remove Mn oxides in
102 possible micro-fractures and other potential labile contaminants. The samples were then
103 repeatedly washed ultrasonically in 18 megohm Milli-Q water before digestion. The
104 method of rock digestion and Hf separation follows those of Yang et al. (2010). Hf isotopic
105 analysis was done using a Neptune MC-ICP-MS in the Institute of Geology and
106 Geophysics, Chinese Academy of Sciences (IGGCAS). The analytical details for Hf
107 isotopic measurements are given by Li et al. (2005). Hf isotopic compositions were
108 normalized to $^{179}Hf/^{177}Hf=0.7325$. In our analysis, we measured $^{176}Hf/^{177}Hf$ values for
109 USGS reference rock standards W-2 (0.282711±0.000013 vs. reference value:
110 0.282715±0.000030, Le Fèvre and Pin, 2001), BHVO-2 ($^{176}Hf/^{177}Hf=0.283082±0.000010$
111 vs. reference value: 0.283096±0.000020, Weis et al., 2005) and BCR-2
112 ($^{176}Hf/^{177}Hf=0.282858±0.000009$ vs. reference value: 0.282870±0.000008, Weis et al.,
113 2007). We also measured the in-house standard Alfa Aesar hafnium solution produced by
114 Johnson Matthey Company (i.e. Alfa Hf, 10000 μg/ml, stock No. 14374, plasma standard
115 solution) (Wu et al., 2006, 2007; Yang et al., 2007). The measured value for Alfa Hf gave

an average $^{176}Hf/^{177}Hf$ of 0.282181±0.000010 (2σ, n=7) (reference value: 0.282189±0.000019, Wu et al., 2006). All of these are indistinguishable from their reference values within analytical errors.

3. Results

The Hf isotope data are given in Table 1 and presented in Fig. 2. The ε_{Hf} are calculated using $([^{176}Hf/^{177}Hf]_{sample}/[^{176}Hf/^{177}Hf]_{CHUR}-1)\times 10000$ (the subscript sample and CHUR denote the value of samples and chondrite), in which, $[^{176}Hf/^{177}Hf]_{CHUR}$ = 0.282772 (Blichert-Toft and Albarède, 1997). The ε_{Nd} values are calculated in the same manner, and the $[^{143}Nd/^{144}Nd]_{CHUR}$ =0.512638 (Dickin, 1997). The ε_{Hf} values for seamount lavas vary from 15.61 to 6.86. The ε_{Hf} and ε_{Nd} correlate well (see Fig. 2), giving a linear expression of $\varepsilon_{Hf}=1.72\varepsilon_{Nd}-2.83$ with $R^2=0.91$. This slope is significantly similar to, although slightly shallower than the mantle array defined by MORB and OIB (i.e., $\varepsilon_{Hf}=1.59\varepsilon_{Nd}+1.28$, Chauvel et al., 2008). The Hf and Nd isotope analyzed in this study cover the range defined by previous analyses of northern EPR MORB (Salters et al., 2011 and reference therein), and more enriched than MORB from southern EPR (Fig. 2). The large range of isotopic variability of the near-EPR seamount lavas suggests that the scale of mantle source heterogeneities may be as small as a few kilometers or even smaller, as recognized previously (e.g., Batiza and Vanko, 1984; Niu and Batiza, 1997). Large variety in compositions for lavas from seamount located at 12°45′N of EPR also implied that the upper mantle is extremely heterogeneous on the scale of a single seamount (Brandl et al., 2012). It is worthy to note that the HIMU-like samples (R78-5-1 and R83-2, shown in green circles in Fig. 2), are offset from the other samples. It is most likely that some mantle source

heterogeneities exist on a small scale and the enriched component may have different origins and, thus, possess different isotopic signatures (Niu et al., 1999, 2002).

4. Discussion

4.1 The effects of fractional crystallization

The major element compositions had been published previously (Niu et al., 2002). The low Mg# values (70 to 52) indicate that none are likely to represent primary melts in equilibrium with mantle olivine (Fo = 89), and all have probably undergone some degree of crystal fractionation. However, the large variations in major and trace element are difficult to explain by fractional crystallization. Additionally, the correlations between isotope compositions and incompatible trace element ratios, and major and trace element concentrations (Fig. 3, and 4) are also inconsistent with closed system crystal fractionation. Other processes other than fractional crystallization must be responsible for variation in composition of most seamount lavas. Considering the composition of seamount lavas is similar to, and more primitive than axial lavas, the crustal contamination is also negligible.

4.2 Melting of two component mantle

4.2.1 Evidence for melting of a component source

Our new Hf isotopic data correlate with Sr, Nd, and Pb isotopes, with ratios of incompatible elements (Fig. 4) and with the abundances of major-trace elements (Fig. 3). Previous studies also showed that the Sr-Nd-Pb isotopic data of these samples correlate with each other, with ratios of incompatible elements and with the abundances and ratios of major elements (Niu and Batiza, 1997; Niu et al., 1999, 2002). The large variation in major-trace element and isotope and the correlations are result from source heterogeneity

and easily explained by mixing between enriched melt (lower MgO, $^{143}Nd/^{144}Nd$, $^{176}Hf/^{177}Hf$, higher incompatible element concentrations and $^{87}Sr/^{86}Sr$ ratios) and relatively depleted melt. Simple mixing of melts derived from lithologically distinct enriched and depleted mantle in variable proportions will result in linear arrays in element-element diagrams, and in all ratio-ratio diagrams in which the denominator element is the same (i.e., A/X vs. B/X diagram) (Langmuir et al., 1978). For the same reason, melting of a source composed of two different lithologies, which are mixed in variable proportions (mixing of sources) but melt to the same extent, also give a straight mixing line. However, the seamount data in this study define curved arrays (Fig. 5), which is inconsistent with the above mentioned mixing. Similar curved arrays have been reported for lavas from the fossil Galapagos Rise (Haase et al., 2011) and seamounts east of the EPR at 12°45′N (Brandl et al., 2012). Variable degrees melting of a two-component mantle in which different lithologies have different trace element and isotope compositions but also different melting behavior may account for the chemical and isotopic variation (Niu and Batiza, 1997; Niu et al., 1999, 2002; Paulick et al., 2010; Haase et al., 2011; Brandl et al., 2012). This concept emphasizes the physical state of a mantle with enriched component as easily melted domains in a more depleted matrix. Increasing evidence suggested that the upper mantle source of oceanic basalts consists of relatively fertile and more refractory lithologies. They have different solidus temperatures and thus begin melting at different depths during adiabatic upwelling. The most important assumption is that the enriched mantle lithologies have lower solidus temperature than the more depleted matrix, thus are preferentially tapped at low degrees of melting (Sleep, 1984; Prinzhofer et al., 1989; Ito and Mahoney, 2005). It is evidenced by the clinopyroxenes in residual abyssal peridotites tend to have more radiogenic Nd isotope than lavas from the same section of ridge, indicating a preferential melting of eclogite or

186 pyroxenite with lower Sm/Nd and $^{143}Nd/^{144}Nd$ ratios during decompression melting
187 (Salters and Dick, 2002). Melting of the fertile lithologies would extract heat from the more
188 refractory matrix, and inhibit the melting of the latter; once the more refractory lithologies
189 begin to melt, the remaining fertile materials may stop melting (Phipps Morgan, 2001), and
190 the melting paths may be curved.

191 There have been several attempts to quantify the range in melt compositions produced
192 by melting of two-component mantle (Ito and Mahoney, 2005; Phipps Morgan, 2001;
193 Phipps Morgan and Morgan, 1999; Stracke and Bourdon, 2009). The contribution of fertile
194 lithologies decreased with the increasing degrees of melting, and lavas produced at lower
195 degree of melting are expected to have higher incompatible element concentrations, higher
196 $^{87}Sr/^{86}Sr$, and lower $^{143}Nd/^{144}Nd$ ratios (e.g., Stracke and Bourdon, 2009).

197 In the following section, the melting model of Stracke and Bourdon (2009) was used
198 to quantitatively model the melt compositions derived from melting of a two-component
199 mantle, in order to investigating the effects of varying solidus temperature, initial
200 proportion of each component, and compositions f of both endmembers, and constraining
201 the mantle heterogeneity beneath the EPR.

202 4.2.2 Quantitative modeling of the melting process

203 The trace-elemental and isotopic compositions, melting behavior, and initial
204 proportion ratio of each component all play an important role in determining melt
205 compositions. Here we assume the simplest case of a two-component mantle, consisting of
206 a volumetrically minor enriched component dispersed in the depleted peridotite matrix.
207 The initial proportion of enriched component is assumed to be no more than 10%. These
208 two components have different solidus temperatures and thus begin melting at different

depths during upwelling. Peridotite melting is assumed to start at ~2.5 GPa, and the beginning depth of the enriched component melting is significantly deeper than to similar to that of peridotite melting (Stracke and Bourdon, 2009). Mineral modes and partition coefficients are given in Appendix 1.

The origin of enriched component is unclear, but likely result from subduction and recycling of oceanic crust, sediments, metasomatised oceanic lithosphere or mantle wedge material (e.g., Hofmann and White, 1982; Niu and O'Hara, 2003; Donnelly et al., 2004).

Recycled ancient oceanic crust might be the enriched component (i.e., ROC model) (e.g., Hofmann and White, 1982), although Niu and O'Hara (2003) suggested that oceanic crust is isotopically too depleted. As a variant of the ROC model, Donnelly et al. (2004) suggested that low-degree melts of subducted oceanic crust could metasomatize the overlying mantle wedge, and the metamomatized mantle wedge could recycle by mantle convection to the ridge supplying enriched MORB (E-MORB) source. One difficulty with the model is that the cold oceanic crust that has undergone dehydration may be too refractory to melt at subduction zone. Another problem is that mantle convection model (Hofmann, 1997; Tolstikhin et al., 2006) may not support this scenario, and the mantle wedge "corner flow" (Niu, 2005) is blocked by the subducting slab, thus, it is difficult for the metasomatized mantle wedge to reach the ocean ridge. Terrigenous sediments may provide enriched composition to depleted mantle (DM) source because few OIB source may have a component of subducted terrigenous sediments (Jackson et al., 2007; Mahoney et al., 1995). However, continental crust (CC) and global subducting sediments (GLOSS) are characterized by depletions in Nb, Ta, P and Ti and enrichment in Pb (Plank and Langmuir, 1998; Rudnick and Gao, 2003). Such a "CC-like signature" is so strong that it

232 should be inherited in the incompatible element characteristics of OIB and E-MORB if
233 terrigenous sediments were indeed the enriched component of DM (Niu et al., 2012).
234 However, it is not observed in global oceanic basalts except for two OIB suites (Jackson et
235 al., 2007; Mahoney et al., 1995). Furthermore, there is no convincing evidence that the
236 terrigenous sediments are the geochemically enriched components of DM on global scale.
237 Recycled metasomatized oceanic lithospheric mantle (ROLM) had also been proposed as
238 a possible enriched component (Niu, 2008, 2009; Niu and O'Hara, 2003, 2009; Niu et al.,
239 2011, 2012). The deep portion of oceanic lithospheric mantle can be enriched in terms of
240 incompatible elements throughout its long histories through mantle metasomatism by low-
241 degree melt. The melt collects atop the seismic low velocity zone (LVZ), and then
242 percolates through and metasomatizes the growing lithosphere via basal accretion. The
243 percolating/metasomatizing Low-degree melt can precipitate mineral phases (e.g.,
244 amphiboles; "macroscopic metasomatism") before finally absorbed ("cryptic
245 metasomatism") in the lithosphere, generating metasomatically veined mantle (e.g., Niu,
246 2008).

247 No matter what the enriched component is (recycled crust or lithospheric mantle), the
248 complex process (i.e., melting, metasomatism, and dehydration during subduction) that
249 they had undergone would increase difficulties in determining their initial trace-element
250 and isotopic compositions. Nevertheless, previous research suggested that the enriched
251 endmember of MORBs array in Hf-Nd isotopic diagram tends to plot either within or in
252 the extension of the OIB array, and none of them towards the HIMU component (Salters et
253 al., 2011). Thus, the previous published trace element and isotope compositions of
254 pyroxenite (recycled MORB), EM1 and EM2 were used to represent that of the enriched

component in the modeling. The isotopic compositions of pyroxenite, EM1 and EM2 are from Ito and Mahoney (2005). And the trace element compositions of pyroxenite, EM1 and EM2 are from Stracke and Bourdon (2009), Willbold and Stracke (2006), and Workman et al. (2004), respectively.

The compositions of depleted endmember are generally estimated from the compositions of oceanic basalts and abyssal peridotites. Actually, the estimated compositions of depleted MORB mantle (DMM) based on that of abyssal peridotites might more faithfully reflect the characteristics of depleted upper mantle due to that the enriched component had been exhausted. And the MORBs, including the most depleted Garrett Transform lavas, are enriched than depleted endmember (discussed below). It is supported by the abyssal peridotites that components of the upper mantle beneath spreading ridges, which have more radiogenic Nd and Hf isotope compositions than those of lavas from the ridge (Salters and Dick, 2002; Stracke et al., 2011).Thus, the estimated composition of DMM mantle based on numerous abyssal peridotites following Workman and Hart (2005) were used here as the depleted endmember in the modeling. The assumption may or may not be realistic, however, it is reasonable. Further researches are needed to better constrain the compositions of depleted/enriched endmembers.

The results of fractional melting model following Stracke and Bourdon (2009) are shown in Figures 5-7. The enriched components are assumed to preferentially melting than the more depleted matrix. The parameters used in the modeling are summarized in Appendix 1. The compositions, mineralogy, melting behavior, and proportion of both components must be more various than that used in the modeling, however, the melting curves still provide important clues on melting of a heterogeneous mantle that composed

278 of at least two component (i.e., enriched and depleted component). Then, the effects of
279 different variables on melt compositions would be discussed below.

280 The melting modeling can broadly reproduce the range in compositions of the
281 seamount lavas in this study (Fig. 5, 6, 7). In the La/Nd versus Yb/Nd and La/Yb versus
282 Sm/Yb diagram (Fig. 5), variable degrees of melting of a heterogeneous mantle fits the
283 curved array defined by EPR seamount lavas that mentioned above, which is contrast with
284 the linear arrays of simple mixing. The melting curves have similar trend, however, the
285 "pyroxenite" endmember fits best to the seamount data in this study and also the previous
286 published axial MORB from EPR 5-15°N. The deviation of "EMI" trajectory from the
287 seamount data, especially in Fig. 5b, is most likely result from the extremely higher
288 incompatible element concentration and the higher degree of fractionation between LREEs
289 and HREEs in "EMI" source. Meanwhile, the degree of enrichment in incompatible
290 element increased with the increasing incompatibility. Consequently, the "EMI"
291 endmember is too enriched to fits the seamount lava in Fig. 5b, although the incompatible
292 element concentration decreased dramatically with the increasing degrees of melting.
293 Previous researches suggested that the curvature of melt curves increased with the
294 increasing proportion of enriched endmember relative to depleted endmember (See Figure
295 8c in Brandl et al., 2012). And increasing in enriched component/depleted component ratio
296 may lead the EMI endmember better fits the seamount data in Fig. 5a, however, it is invalid
297 in Fig. 5b.

298 The effects of difference in solidus temperatures between the two endmembers on
299 melt compositions were shown in Fig. 6. Peridotite melting is assumed to start at ~2.5 GPa
300 (Stracke and Bourdon, 2009). And the melt evolutionary paths that the beginning depth of

301 the enriched component melting is assumed to be similar to and significantly deeper than
302 that of peridotite melting were exhibited in solid lines and dashed lines, respectively. The
303 largest melt heterogeneity in the ratios of trace element is observed for small differences in
304 solidus temperature between the two components (Fig. 6). If the contrast in solidus
305 temperature is too large, the enriched component would be completely exhausted before
306 peridotite melting, and the clear correlations between trace element and isotope ratios of
307 the seamount lavas in this study would not be observed in the pooled melts (Fig. 6). The
308 seamount data lies between the melt curves at different solidus temperatures, and "EM1
309 /EM2" endmember, especially in condition that the solidus temperatures of the two
310 endmembers are similar, could better reproduce the seamount data. The "pyroxenite"
311 endmember is significantly depleted in Sr isotope than the enriched seamount lavas (Fig.
312 6b), indicating that "pyroxenite" endmember is not a reasonable enriched component or
313 other enriched components must also involve in the source. The melting modeling in
314 correlations between Sr-Nd-Pb isotopes further supported that the enriched component
315 might be complex, and it is most likely composed of EM1 and/or pyroxenite (Fig. 7). Melt
316 compositions in assumption that the initial proportion of EM1 and pyroxenite is 0.06 and
317 0.04, respectively, can match well with the isotopic compositions of seamount lavas (Fig.
318 7b, c).
319 In summary, the large variation in trace element ratios (e.g., La/Sm and Nb/Zr) and
320 isotope of seamount lavas in this study and the correlations between them is the result of
321 melting of a heterogeneous mantle. And "EM1" and/or "pyroxenite" as the enriched
322 component could better fits the seamount data and axial MORB from EPR at 5-15°N both
323 in trace element and isotope compositions in the modeling. Thus, we infer that the

metasomatized lithospheric mantle and/or oceanic crust might be the reasonable enriched component in mantle source beneath northern EPR. The parameters used in the modeling should be further constrained.

Furthermore, the most depleted seamount lavas in this study and previous published axial MORB from northern EPR approximate to the depleted endmember, however, it is enriched than the mantle source. Previous researches also suggested that the average incompatible trace element and isotope composition of mantle source is significantly more depleted than mantle-derived magmas (e.g., Stracke and Bourdon, 2009; Brandl et al., 2012). Oceanic basalts were often used to infer the composition of the upper mantle. However, if melting of two-component mantle is common and an important process, then the studies of oceanic basalts that assume that the isotope compositions of basalts are identical to those of their mantle source might be wrong.

4.3 Implications for Hf-Nd isotopic variations on a global scale

Previous studies show that there is a good correlation between Hf and Nd isotope for global MORBs (e.g., Chauvel et al., 2008; Vervoort et al., 2011). However, a later comprehensive study of MORBs (Salters et al., 2011) shows that the ε_{Hf} values of global MORBs varies widely at given ε_{Nd} value. Here we use $\Delta\varepsilon_{Hf}$ values to describe the derivation of the measured ε_{Hf} value from that of the mantle array defined by Chauvel et al. (2008), i.e., $\varepsilon_{Hf}=1.59\varepsilon_{Nd}+1.28$. It is obvious that the $\Delta\varepsilon_{Hf}$ values of Pacific MORBs, Atlantic MORBs and Indian MORBs are different (Fig. 8b). In general, MORBs and seamount lavas of Pacific spreading centers have the lowest and relatively constant $\Delta\varepsilon_{Hf}$ values (Fig. 8). However, Atlantic and Indian MORBs range widely in $\Delta\varepsilon_{Hf}$ values, and the

347 Atlantic MORBs, especially the North Atlantic MORBs, have the highest $\Delta\varepsilon_{Hf}$ values (Fig.
348 8). The fundamental reason must be the global scale heterogeneity of DMM, i.e., the large
349 variations in $\Delta\varepsilon_{Hf}$ values are most likely dominated by local variations of source
350 compositions. The above discussed fractional melting modeling of a heterogeneous mantle
351 also supported that the isotopic composition of melt is mainly controlled by source
352 compositions, melting behavior and initial proportion of each component. Addition of a
353 component with high $\Delta\varepsilon_{Hf}$ values to the mantle source might lead the melt towards high
354 $\Delta\varepsilon_{Hf}$ values on different extent. The mantle component with high ε_{Hf} value is most likely to
355 be the residues of ancient melting events with garnet present as a residual phase. The
356 partition coefficients of Lu between garnet and basaltic liquids is much higher than that of
357 Hf (i.e., $D_{Lu}/D_{Hf}>>1$), and the residues produced by melt extraction at great depth where
358 garnet is stable and as a residual phase of the source would impart an elevated Lu/Hf ratios
359 and evolve to high $^{176}Hf/^{177}Hf$ in the residues if the partial melting event is ancient (e.g.,
360 Schmidberger et al. 2002). Salters et al. (2011) proposed that various amounts of residual
361 oceanic lithosphere (ReLish) can account for the variation in ε_{Hf} value at constant Nd
362 isotope. And the amount of ReLish that contributes to the Pacific MORB was suggested to
363 be relatively constant and that various widely as to Atlantic and Indian MORBs (Salters et
364 al., 2011). The more uniform $\Delta\varepsilon_{Hf}$ value of Pacific MORB may also simply reflect the fact
365 that melt mixing in magma chambers at fast-spreading ridges is more efficient (Rubin and
366 Sinton, 2007).
367 Alternatively, the sub-continental lithospheric mantle (SCLM) was also proposed to
368 be a suitable component to produce the high Hf isotope of lavas from Lucky Strike Ridge
369 that along the northern Mid-Atlantic Ridge (Hamelin et al., 2013). The Pacific spreading

center is always suggested to be ancient and not associated with the continental rifting, thus, the continental lithospheric mantle is absent or exhausted. In contrast, the opening time of Atlantic and Indian spreading center is no longer than 200 Ma, and the continental lithospheric mantle that detached into the upper mantle can feed the MORB source. It had been approved that the continental materials could introduce into the Atlantic-Indian upper mantle during continental rifting (e.g., Torsvik et al., 2013). Furthermore, ancient depleted continental lithospheric mantle with extremely radiogenic Hf isotopes had been observed (Schmidberger et al., 2002; Bedini et al., 2004; Simon et al., 2007; Chu et al., 2009). Although the Hf and Nd isotopic compositions of SCLM range widely from negative to positive values, most of them have extremely high ε_{Hf} value (even to +200) (Fig. 8) that can interpret the lowest and relatively constant $\Delta\varepsilon_{Hf}$ values for Pacific MORBs and largely various and higher $\Delta\varepsilon_{Hf}$ values for Atlantic and Indian MORBs.

4.4 Pseudochron ages

Fig. 9 shows that our samples give Rb-Sr, Sm-Nd and Lu-Hf pseudochron ages of 182±33 Ma, 276±50 Ma and 387±93 Ma, respectively. The ages have been reported at other locations of ocean ridge and nearby seamounts (Donnelly et al., 2004; Niu et al., 1996; Zindler et al., 1984). Zindler et al. (1984) suggested that the Sm-Nd pseudochrons of near-EPR seamounts have age significance and interpreted that to be controlled by (1) the position of depleted and enriched end-member in $^{143}Nd/^{144}Nd$ vs. Sm/Nd space and (2) independent magma source of two end-members. The Rb-Sr and Sm-Nd pseudochron ages of near-EPR seamounts (187 Ma and 238 Ma, respectively) are similar to our results, which were interpreted to provide constraints on the origin and timing of E-MORB source enrichment (Donnelly et al., 2004). However, Niu et al. (1996) suggested that these

pseudochrons are statistically significant mixing trends without chronological significance.

These ages shown by different radioactive decay systems are non-conformable, suggesting indeed that the "ages" are of no chronological significance, but are best explained as results of melting-induced mixing with the pseudochron slopes controlled by the compositions of the enriched component and the depleted end-member. The fractional melting modeling can reproduce the arrays to a first order (Fig. 9) with the "EM1" endmember fits the seamount data better. It is consistent with the above conclusion that "EM1" is a possible origin of enriched component. The source mantle contains a volumetrically minor enriched component, and with increasing degree of melting, the contribution to the pooled melt from the more fertile component with higher Rb/Sr, $^{87}Sr/^{86}Sr$, and lower Sm/Nd, Lu/Hf, $^{143}Nd/^{144}Nd$, $^{176}Hf/^{177}Hf$ ratios progressively decreases.

5. Conclusions

1. New Hf isotopic data of basaltic glasses from seamounts flanking the EPR between 5° and 15°N demonstrate that Hf and Nd isotope of these lavas are correlated and form a well-defined trend that parallel to the mantle array.

2. The correlated Hf-Nd isotopic variations, together with their correlations with Sr-Pb isotope as well as with abundances and ratios of incompatible elements, suggest that the geochemistry of EPR and near-EPR seamount lavas is most consistent with melting-induced mixing of a two-component mantle (i.e., an easily-melted enriched component dispersed in the more depleted refractory matrix).

3. Fractional melting modeling of a heterogeneous mantle can reproduce the variations in trace-element and isotope compositions of seamount lavas. "Pyroxenite"

and/or EM1 endmember better fits the data, indicating that the enriched component is most likely to be recycled oceanic crust or metasomatized oceanic lithospheric mantle.

4. The contribution of residual continental lithospheric mantle may interpret the difference in $\Delta\varepsilon_{Hf}$ values between Pacific, Atlantic and Indian MORBs.

5. The Rb-Sr, Sm-Nd and Lu-Hf pseudochrons have no age significance, but are mixing lines constrained by the composition of the enriched component and the depleted end-member.

Acknowledgements

Y.H. Yang and J.Y. Chen are thanked for their help during the chemical separation and analyses. We thank C. Chauvel, P. Mueller, J. Blichert-Toft, C.L. Waters, A. Stracke and V.G.M. Salters for their constructive suggestions for this paper. A. Stracke and J. Phipps Morgan are appreciated for help in quantitatively modeling. This study is supported by the National Natural Science Foundation of China (Grants 41273013, 41130314, 91014003), China Postdoctoral Science Foundation, Specialized Research Fund for the Doctoral Program of Higher Education of China (2012021110021), Scientific Research Foundation of Shandong University of Science and Technology for Recruited Talents (2016RCJJ008).

References

Agranier, A., Blichert-Toft, J., Graham, D., Debaille, V., Schiano, P., Albarede F., 2005. The spectra of isotopic heterogeneities along the mid-Atlantic Ridge. Earth Planetary Science Letters 238, 96-109.

Allègre, C., Turcotte, D., 1986. Implications of a two-component marble-cake mantle. Nature 323, 123-127.

Amante, C., Eakins B.W., 2009. ETOPO1 1 Arc-Minute Global Relief Model: Procedures, Data Sources and Analysis. NOAA Technical Memorandum NESDIS NGDC-24, 1-19.

Arevalo Jr., R., McDonough, W.F., 2010. Chemical variations and regional diversity observed in MORB. Chemical Geology 271, 70–85.

Batiza, R., Niu, Y.L., 1992. Petrology and magma chamber processes at the East Pacific Rise ~9°30′ N. Journal of Geophysical Research 97, 6779-6797.

Batiza, R., Niu, Y.L., Zayac, W.C., 1990. Chemistry of seamounts near the East Pacific Rise implications for the geometry of sub-axial mantle flow. Geology 18, 1122-1125.

Batiza, R., Vanko, D., 1984. Petrology of Young Pacific Seamounts. Journal of Geophysical Research 89, 11235-11260.

Bedini, R. M., Blichert-Toft, J., Boyet, M., Albarède F., 2004. Isotopic constraints on the cooling of the continental lithosphere. Earth and Planetary Science Letters 223(1–2), 99-111.

Bianchini, G., Beccaluva, L., Bonadiman, C., Nowell, G., Pearson, G., Siena, F., Wilson, M., 2007. Evidence of diverse depletion and metasomatic events in harzburgite–lherzolite mantle xenoliths from the Iberian plate (Olot, NE Spain): Implications for

458 lithosphere accretionary processes. Lithos 94, 25-45.
459 Blichert-Toft, J., 2001. On the Lu-Hf isotope geochemistry of silicate rocks. Geostandard
460 Newsletter 25, 41-56.
461 Blichert-Toft, J., Agranier, A., Andres, M., Kingsley, R., Schilling, J.G., Albarède, F., 2005.
462 Geochemical segmentation of the Mid-Atlantic Ridge north of Iceland and ridge-hot
463 spot interaction in the North Atlantic. Geochemistry, Geophysics, Geosystems 6,
464 Q01E19, doi:10.1029/2004GC000788.
465 Blichert-Toft, J., Albarède, F., 1997. The Lu-Hf isotope geochemistry of chondrites and
466 the evolution of the mantle-crust system. Earth Planetary Science Letters 148, 243-
467 258.
468 Brandl. P.A., Beier, C., Regelous, M., Abouchami, W., Haase, K. M., Garbe-Schönberg,
469 D., Galer, S.J.G., 2012. Volcanism on the flanks of the East Pacific Rise: Quantitative
470 constraints on mantle heterogeneity and melting processes. Chemical Geology 298-
471 299, 41-56.
472 Carlson, R.W., Irving, A.J., Schulzec, D.J., Hearn Jr, B.C., 2004. Timing of Precambrian
473 melt depletion and Phanerozoic refertilization events in the lithospheric mantle of the
474 Wyoming Craton and adjacent Central Plains Orogen. Lithos 77, 453- 472.
475 Chauvel, C., Blichert-Toft, J., 2001. A hafnium isotope and trace element perspective on
476 melting of the depleted mantle. Earth Planetary Science Letters 190, 137-151.
477 Chauvel, C., Lewin, E., Carpentier, M., Arndt, N.T., Marini, J.C., 2008. Role of recycled
478 oceanic basalt and sediment in generating the Hf-Nd mantle array. Nature Geoscience
479 1, 64-67.
480 Chu, Z.Y., Wu, F.Y., Walker, R.J., Rudnick, R.L., Pitcher, L., Yang, Y.H., A.W.S., 2009.

481 Temporal evolution of the lithospheric mantle beneath the eastern North China Craton.
482 Journal of Petrology 50, 1857-1898.
483 Debaille, V., Blichert-Toft, J., Agranier, A., Doucelance, R., Schiano, P., Albarède, F.,
484 2006, Geochemical component relationships in MORB Mid-Atlantic Ridge, 22-35°N.
485 Earth Planetary Science Letters 241, 844-862.
486 Dickin, A.P., 1997. Radiogenic Isotope Geology, second ed. Cambridge University Press,
487 New York.
488 Donnelly, K.E., 2002. The Genesis of E-MORB: Extensions and Limitations of the Hot
489 Spot Model (PhD thesis), Columbia University, New York.
490 Donnelly, K.E., Goldstein, S.L., Langmuir, C.H., Spiegelman, M., 2004. Origin of
491 enriched ocean ridge basalts and implications for mantle dynamics. Earth Planetary
492 Science Letters 226, 347-366.
493 Dosso, L., Bougault, H., Joron, J.L., 1993. Geochemical morphology of the North Mid-
494 Atlantic Ridge, 10°-24°N: Trace element-isotope complementarity. Earth Planetary
495 Science Letters 120, 443-462.
496 Douglass, J., Schilling, J.G., 1999. Plume-ridge interactions of the Discovery and Shona
497 mantle plumes with the southern Mid-Atlantic Ridge (40°-50°S). Journal of
498 Geophysical Research 104, 2941-2962.
499 Faure, G., 1986. Principles of Isotope Geology, second ed. John Wiley & Sons, New York.
500 Fontignie, D. Schilling, J.G., 1996. Mantle heterogeneities beneath the South Atlantic: a
501 Nd-Sr-Pb isotope study along the Mid-Atlantic Ridge (3°S-46°S). Earth Planetary
502 Science Letters 142, 209-221.
503 Gale, A., Dalton, C., Langmuir, C.H., Su, Y., Schilling, J.G, 2013. The mean composition

of ocean ridge basalts. Geochemistry Geophysics Geosystems 14, 489-518.

Gast, P.W., Tilton, G.R., Hedge, C., 1964. Isotopic composition of lead and strontium from Ascension and Gough Islands. Science 145, 1181-1185.

Graham, D.W., Blichert-Toft, J., Russo, C.J., Rubin, K.H., Albarède, F., 2006. Cryptic striations in the upper mantle revealed by hafnium isotopes in southeast Indian ridge basalts. Nature 440, 199-202.

Haase, K.M., Regelous, M., Duncan, R., Brandl, P. A., Stroncik, N., Grevemeyer, I., 2011. Insights into mantle composition and mantle melting beneath mid-ocean ridges from post-spreading volcanism on the fossil Galapagos Rise. Geochemistry, Geophysics, Geosystems 12.

Hamelin, C., Dosso, L., Hanan, B.B., Moreira, M., Kositsky, A.P., Thomas, M.Y., 2011. Geochemical portray of the Pacific Ridge: New isotopic data and statistical techniques. Earth Planetary Science Letters 302, 154-162.

Hanan, B.B., Blichert-Toft, J., Pyle, D.G., Christie, D.M., 2004. Contrasting origins of the upper mantle revealed by hafnium and lead isotopes from the Southeast Indian Ridge. Nature 432, 91-94.

Hirschmann, M., Stolper, E., 1996. A possible role for garnet pyroxenite in the origin of the 'garnet signature' in MORB. Contributions to Mineralogy and Petrology 124, 185-208.

Hofmann, A.W., 1997. Mantle geochemistry: The message from oceanic volcanism. Nature 385, 219-229.

Hofmann, A.W., White, W.M., 1982. Mantle plumes from ancient oceanic crust. Earth Planetary Science Letters 57, 421-436.

527 Ito, G., Mahoney, J. J., 2005. Flow and melting of a heterogeneous mantle: 1. Method and
528 importance to the geochemistry of ocean island and mid-ocean ridge basalts. Earth
529 and Planetary Science Letters 230, 29-46.
530 Jackson, M.G., Hart, S.R., Koppers, A.A.P., Staudigel, H., Konter, J., Blusztajn, J., Kurz,
531 M., Russell, M.A., 2007. The return of subducted continental crust in Samoan lavas.
532 Nature 448, 684-687.
533 Janney, P.E., Le Roex, A.P., Carlson, R.W., 2005. Hafnium isotope and trace element
534 constraints on the nature of mantle heterogeneity beneath the Central Southwest
535 Indian Ridge (13°E to 47°E). Journal of Petrology 46, 2427-2464.
536 Johnson, C.M., Beard, B.L., 1993. Evidence from hafnium isotopes for ancient sub-oceanic
537 mantle beneath the Rio Grande rift. Nature 362, 441-444.
538 Kemp, A.I.S., Hawkesworth, C.J., Paterson, B.A., Kinny, P.D., 2006. Episodic growth of
539 the Gondwana supercontinent from hafnium and oxygen isotopes in zircon. Nature
540 439, 580-583.
541 Kempton, P.D., Fitton, J.G., Saunders, A.D., Nowell, G.M., Taylor, R.N., Hardarson, B.
542 S., Pearson, G., 2000. The Iceland plume in space and time: a Sr-Nd-Pb-Hf study of
543 the North Atlantic rifted margin. Earth Planetary Science Letters 177, 255-271.
544 Kempton, P.D., Pearce, J.A., Barry, T.L., Fitton, J.G., Langmuir, C., Christie, D.M., 2002.
545 Sr-Nd-Pb-Hf Isotope Results from ODP Leg 187: Evidence for Mantle Dynamics of
546 the Australian-Antarctic Discordance and Origin of the Indian MORB Source.
547 Geochemistry, Geophysics, Geosystems 3, 1074, doi:10.1029/2002GC000320.
548 Klein, E.M., Langmuir, C.H., Zindler, A., Staudigel, H., Hamelin, B., 1988. Isotope
549 evidence of a mantle convection boundary at the Australian-Antarctic Discordance.

Nature 333, 623-629.

Langmuir, C., Vocke Jr., R., Hanson, G., Hart, S., 1978. A general mixing equation with applications to Icelandic basalts. Earth and Planetary Science Letters 37, 380-392.

Lapen, T.J., Medaris Jr, G.L., Johnson, C.M., Beard, B.L., 2005. Archean to Middle Proterozoic evolution of Baltica subcontinental lithosphere: Evidence from combined Sm-Nd and Lu-Hf isotope analyses of the Sandvik ultramafic body, Norway. Contributions to Mineralogy and Petrology 150, 131-145.

Le Fèvre, B., Pin, C., 2001. An Extraction Chromatography Method for Hf Separation Prior to Isotopic Analysis Using Multiple Collection ICP-Mass Spectrometry. Analytical Chemistry 73, 2453-2460.

Li, X.H., Qi, C.S., Liu, Y., Liang, X.R., Tu, X.L., 2005. Rapid separation of Hf from rock samples for isotope analysis by MC-ICPMS, a modified single-column extraction chromatography method. Geochimica 34, 110-114. (in Chinese with English abstract)

Mahoney, J.J., Graham, D.W., Christie, D.M., Johnson, K.T.M., Hall, L.S., Vonderhaar, D.L., 2002. Between a hotspot and a cold spot: Isotopic variation in the Southeast Indian Ridge asthenosphere, 86°E-118°E. Journal of Petrology 43, 1155-1176.

Mahoney, J.J., Jones, W.B., Frey, F.A., Salters, V.J.M., Pyle, D.G., Davies, H.L., 1995. Geochemical characteristics of lavas from Broken Ridge, the Naturaliste Plateau and southernmost Kerguelen Plateau: Oceanic plateau volcanism in the southeast Indian Ocean. Chemical Geology 120, 315-345.

Meyzen, C.M., Blichert-Toft, J., Ludden, J.N., Humler, E., Mével, C., Albarède, F., 2007. Isotopic portrayal of the Earth's upper mantle flow field. Nature 447, 1069-1074.

Niu, Y.L., 2005. Generation and evolution of basaltic magmas: some basic concepts and a

573 new view on the origin of Mesozoic-Cenozoic basaltic volcanism in eastern China.
574 Geological Journal of China Universities 11, 9-46.
575 Niu, Y.L., 2008. The origin of alkaline lavas. Science 320, 883-884.
576 Niu, Y.L., 2009. Some basic concepts and problems on the petrogenesis of intra-plate
577 ocean island basalts (OIB). Chinese Science Bulletin 54, 4148-4160.
578 Niu, Y.L., Batiza, R., 1997. Trace element evidence from seamounts for recycled oceanic
579 crust in the Eastern Pacific mantle. Earth Planetary Science Letters 148, 471-483.
580 Niu, Y.L., O'Hara, M.J., 2003. Origin of ocean island basalts: A new perspective from
581 petrology, geochemistry and mineral physics considerations. Journal of Geophysical
582 Research 108, ECV 5 1-19.
583 Niu, Y.L., O'Hara, M.J., 2009. MORB mantle hosts the missing Eu (Sr, Nb, Ta and Ti) in
584 the continental crust: New perspectives on crustal growth, crust-mantle differentiation
585 and chemical structure of oceanic upper mantle. Lithos 112, 1-17.
586 Niu, Y.L., Collerson, K.D., Batiza, R., Wendt, J.I., Regelous, M., 1999. The origin of E-
587 type MORB at ridges far from mantle plumes: The East Pacific Rise at 11°20′N.
588 Journal of Geophysical Research 104, 7067-7087.
589 Niu, Y.L., Regelous, M., Wendt, I.J., Batiza, R., O'Hara, M.J., 2002. Geochemistry of
590 near-EPR seamounts: importance of source vs. process and the origin of enriched
591 mantle component. Earth Planetary Science Letters 199, 327-345.
592 Niu, Y.L., Waggoner, D.G., Sinton, J.M., Mahoney, J.J., 1996. Mantle source
593 heterogeneity and melting processes beneath seafloor spreading centers: The East
594 Pacific Rise, 18-19°S. Journal of Geophysical Research 101, 27711-27733.
595 Niu, Y.L., Wilson, M., Humphreys, E.R., O'Hara, M.J., 2011. The origin of intra-plate

596 ocean island basalts (OIB): The lid effect and its geodynamic implications. Journal of
597 Petrology 52, 1443-1468.
598 Niu, Y.L., Wilson, M., Humphreys, E.R., O'Hara, M.J., 2012. A trace element perspective
599 on the source of ocean island basalts (OIB) and fate of subducted ocean crust (SOC)
600 and mantle lithosphere (SML). Episodes 35, 310-327.
601 Nowell, G.M., Kempton, P.D., Noble, S.R., Fitton, J.G., Saunders, A.D., Mahoney, J.J.,
602 Taylor, R.N., 1998. High precision Hf isotope measurements of MORB and OIB by
603 thermal ionization mass spectrometry: Insights into the depleted mantle. Chemical
604 Geology 149, 211-233.
605 Parsons, B., Sclater, J.G., 1977. An analysis of the variation of ocean floor bathymetry and
606 heat flow with age. Journal of Geophysical Research 82, 803-827.
607 Patchett, P.J., 1983. Hafnium isotope results from mid-ocean ridges and Kerguelen. Lithos
608 16, 47-51.
609 Patchett, P.J., Tatsumoto, M., 1980. Hafnium variations in oceanic basalts. Geophysical
610 Research Letters 7, 1077-1080.
611 Paulick, H., Münker, C., Schuth, S., 2010. The influence of small-scale mantle
612 heterogeneities on Mid-Ocean Ridge volcanism: Evidence from the southern Mid-
613 Atlantic Ridge (7°30′S to 11°30′S) and Ascension Island. Earth and Planetary Science
614 Letters 296, 299-310.
615 Phipps Morgan, J., 2001. Thermodynamics of pressure release melting of a veined plum
616 pudding mantle. Geochemistry, Geophysics, Geosystems 2, 1001.
617 Phipps Morgan, J., Morgan, W., 1999. Two-stage melting and the geochemical evolution
618 of the mantle: a recipe for mantle plum-pudding. Earth and Planetary Science Letters

170, 215-239.

Pilet, S., Hernandez, J., Sylvester, P., Poujol, M., 2005. The metasomatic alternative for ocean island basalt chemical heterogeneity. Earth and Planetary Science Letters 236, 148-166.

Plank, T., Langmuir, C.H., 1998. The chemical composition of subducting sediment and its consequences for the crust and mantle. Chemical Geology 145, 325-394.

Prinzhofer, A., Lewin, E., Allegre, C. J., 1989. Stochastic melting of the marble cake mantle: Evidence from local study of the East Pacific Rise at 12°50′ N. Earth and Planetary Science Letters 92, 189-206.

Pyle, D., Christie, D.M., Mahoney, J.J., 1992. Resolving an isotopic boundary within the Australian-Antarctic discordance. Earth Planetary Science Letters 112, 161-178.

Rubin, K. H., Sinton, J. M., 2007. Inferences on mid-ocean ridge thermal and magmatic structure from MORB compositions. Earth Planetary Science Letters 260, 257-267.

Rudnick, R.L., Gao, S., 2003. Composition of the continental crust, in: Holland, H.D., Turekian, K.K. (Eds), Treatise on Geochemistry (Vol 3). Elsevier Ltd., Amsterdam, pp. 1-64.

Salters, V.J.M., 1996. The generation of mid-ocean ridge basalts from the Hf and Nd isotope perspective. Earth Planetary Science Letters 141, 109-123.

Salters, V.J.M., Dick, H.J.B., 2002. Mineralogy of the mid-ocean-ridge basalt source from neodymium isotopic composition of abyssal peridotites. Nature 418, 68-72.

Salters, V.J.M., Hart, S.R., 1991. The mantle sources of ocean ridges, islands and arcs: the Hf isotope connection. Earth Planetary Science Letters 104, 364-380.

Salters, V.J.M., Stracke, A., 2004. Composition of depleted mantle. Geochemistry,

642 Geophysics, Geosystems 5, Q05B07, doi:10.1029/2003GC000597.
643 Salters, V.J.M., White, W.M., 1998. Hf isotope constraints on mantle evolution. Chemical
644 Geology 145, 447-460.
645 Salters, V.J.M., Zindler, A., 1995. Extreme $^{176}Hf/^{177}Hf$ in the sub-oceanic mantle. Earth
646 Planetary Science Letters 129, 13-30.
647 Salters, V.J.M., Mallick, S., Hart, S.R., Langmuir, C.E., Stracke, A., 2011. Domains of
648 depleted mantle: New evidence from hafnium and neodymium isotopes.
649 Geochemistry, Geophysics, Geosystems 12, Q08001, doi:10.1029/2011GC003617.
650 Schilling, J., Zapac, M., Evans, R., Johnston, T., White, W. M., Devine, J.D., 1983.
651 Petrologic and geochemical variations along the Mid-Atlantic Ridge from 29°N to
652 73°N. American Journal of Science 283, 510-586.
653 Schilling, J.G., Fontignie, D., Blichert-Toft, J., Kingsley, R., Tomza, U., 2003. Pb-Hf-Nd-
654 Sr isotope variations along the Galápagos Spreading Center (101°-83°W): Constraints
655 on the dispersal of the Galápagos mantle plume. Geochemistry, Geophysics,
656 Geosystems 4, 8512, doi:10.1029/2002GC000495.
657 Schilling, J.G., Hanan, B.B., McCully, B., Kingsley, R.H., Fontignie, D., 1994. Influence
658 of the Sierra Leone mantle plume on the equatorial Mid-Atlantic Ridge: A Nd-Sr-Pb
659 isotopic study. Journal of Geophysical Research 99, 12005-12028.
660 Schilling, J.G., Kingsley, R., Fontignie, D., Poreda, R., Xue, S., 1999. Dispersion of the
661 Jan Mayen and Iceland mantle plumes in the Arctic: A He-Pb-Nd-Sr isotope tracer
662 study of basalts from the Kolbeinsey, Mohns, and Knipovich Ridges. Journal of
663 Geophysical Research 104, 10543-10569.
664 Schmidberger, S. S., Simonetti, A., Francis, D., Gariepy, C., 2002. Probing Archean

665 lithosphere using the Lu-Hf isotope systematics of peridotite xenoliths from Somerset
666 Island kimberlites, Canada. Earth and Planetary Science Letters 197, 245-259.
667 Simon, N.S.C., Carlson, R.W., Pearson, D.G., 2007. The Origin and Evolution of the
668 Kaapvaal Cratonic Lithospheric Mantle. Journal of Petrology 48, 589-625.
669 Sims, K.W.W., Goldstein, S.J., Blichert-Toft, J., Perfit, M.R., Kelemen, P., Fornaril, D.J.,
670 Michael, P., Murrell, M.T., Hart, S.R., Depaolo, D.J., Layne, G., Ball, L., Jull, M.,
671 Bender, J., 2002. Chemical and isotopic constraints on the generation and transport of
672 magma beneath the East Pacific Rise. Geochimica et Cosmochimica Acta 66, 3481-
673 3504.
674 Sleep, N.H., 1984. Tapping of magmas from ubiquitous mantle heterogeneities: an
675 alternative to mantle plumes? Journal of Geophysical Research 89, 10029-10041.
676 Stracke, A., Bourdon, B., 2009. The importance of melt extraction for tracing mantle
677 heterogeneity. Geochimica et Cosmochimica Acta 73, 218-238.
678 Stracke, A., Snow, J.E., Hellebrand, E., von der handt, A., Bourdon, B., Birbaum, K.,
679 Günther, D., 2011. Abyssal peridotite Hf isotopes identify extreme mantle depletion.
680 Earth and Planetary Science Letters 308, 359-368.
681 Tolstikhin, I.N., Kramer, J.D., Hofmann, A.W., 2006. A chemical Earth model with whole
682 mantle convection: The importance of a core-mantle boundary layer (D″) and its early
683 formation. Chemical Geology 226, 79-99.
684 Torsvik, T. H., Amundsen, H., Hartz, E. h., Corfu, F., Kusznir, N., Gaina, G., Doubrovine,
685 P. V., Steinberger, B., Ashwal, L. D., Jamtveit, B., 2013. A Precambrian
686 microcontinent in the Indian Ocean. Nature Geoscience doi:10.1038/NGEO1736.
687 Vervoort, J.D., Patchett, P.J., Blichert-Toft, J., Albarede, F., 1999. Relationships between

688 Lu-Hf and Sm-Nd isotopic systems in the global sedimentary system. Earth Planetary
689 Science Letters 168, 79-99.
690 Vervoort, J.D., Patchett, P.J., Gehrels, G.E., Nutman, A.P., 1996. Constraints on early
691 Earth differentiation from hafnium and neodymium isotopes. Nature 379, 624-627.
692 Vervoort, J.D., Plank, T., Prytulak, J., 2011. The Hf-Nd isotopic composition of marine
693 sediments. Geochimica et Cosmochimica Acta 75, 5903-5926.
694 Weis, D., Kieffer, B., Maerschalk, C., Pretorius, W., Barling, J., 2005. High-precision Pb-
695 Sr-Nd-Hf isotopic characterization of USGS BHVO-1 and BHVO-2 reference
696 materials. Geochemistry, Geophysics, Geosystems 6, Q02002,
697 doi:10.1029/2004GC000852.
698 Weis, D., Kieffer, B., Hanano, D., Silva, I.N., Barling, J., Pretorius, W., Maerschalk, C.,
699 Mattielli, N., 2007. Hf isotope compositions of US Geological Survey reference
700 materials. Geochemistry, Geophysics, Geosystems 8, Q06006,
701 doi:10.1029/2006GC001473.
702 White, W.M., 1985. Sources of oceanic basalts: Radiogenic isotopic evidence. Geology 13,
703 115-118.
704 White, W.M., Hofmann, A.W., 1982. Sr and Nd isotope geochemistry of oceanic basalts
705 and mantle evolution. Nature 296, 821-825.
706 Wittig, N., Baker, J.A., Downes, H., 2007. U–Th–Pb and Lu–Hf isotopic constraints on the
707 evolution of sub-continental lithospheric mantle, French Massif Central. Geochimica
708 et Cosmochimica Acta 71, 1290-1311.
709 Workman, R. K., Hart, S. R., 2005. Major and trace element composition of the depleted
710 MORB mantle (DMM). Earth and Planetary Science Letters 231, 53-72.

711 Wu, F.Y., Li, X.H., Zheng, Y.F., Gao, S., 2007. Lu-Hf isotopic systematics and their
712 applications in petrology. Acta Petrologica Sinica 23, 185-220. (in Chinese with
713 English abstract)
714 Wu, F.Y., Yang, Y.H., Xie, L.W., Yang, J.H., Xu, P., 2006. Hf isotopic compositions of
715 the standard zircons and baddeleyites used in U-Pb geochronology. Chemical
716 Geology 234, 105-126.
717 Yang, Y.H., Zhang, H.F., Chu, Z.Y., Xie, L.W., Wu, F.Y., 2010. Combined chemical
718 separation of Lu, Hf, Rb, Sr, Sm and Nd froma single rock digest and precise and
719 accurate isotope determinations of Lu-Hf, Rb-Sr and Sm-Nd isotope systems using
720 Multi-Collector ICPMS and TIMS. International Journal of Mass Spectrometry 290,
721 120-126.
722 Yang, Y.H., Zhang, H.F., Liu, Y., Xie, L.W., Qi, C.S., Tu, X.L., 2007. One column
723 procedure for Hf purification in geological samples using anion exchange
724 chromatography and its isotopic analyses by MC-ICP-MS. Acta Petrologica Sinica
725 23, 227-232. (in Chinese with English abstract)
726 Yu, D., Fontignie, D., Schilling, J.G., 1997. Mantle plume-ridge interactions in the central
727 North Atlantic: A Nd isotope study of Mid-Atlantic ridge basalts. Earth Planetary
728 Science Letters 146, 259-272.
729 Zindler, A., Hart, S., 1986. Chemical geodynamics. Annual Review of Earth and Planetary
730 Sciences 14, 493-571.
731 Zindler, A., Staudigel, H., Batiza, R., 1984. Isotope and trace element geochemistry of
732 young Pacific seamounts: implications for the scale of upper mantle heterogeneity.
733 Earth Planetary Science Letters 70, 175-195.

Figure captions

Fig. 1 (a) Tectonic framework of the northern (5°-15°N) EPR and vicinity; (b) Simplified map of the study area showing the locations of near-ridge seamounts. The size of the circles (sample locations) are not to scale (Niu and Batiza, 1997; Niu et al., 2002).

Fig. 2 Hf and Nd isotopic variations of seamount lavas on the flanks of the EPR between 5° and 15°N. Nd isotope data are from Niu et al. (2002). The oceanic basalts field, defined by MORBs, OIBs and island arc volcanic rocks (IAVs), is from Chauvel et al. (2008) and Vervoort et al. (1999). The mantle array is according to Chauvel et al. (2008). The field of abyssal peridotite and marine sediments is from Stracke et al. (2011), Vervoort et al. (2011), respectively. The Pacific, Atlantic and Indian MORB data are from Salters et al. (2011), Sims et al. (2002), Blichert-Toft et al. (2005), and Janney et al. (2005). The blue and green circles are alkali basalts and HIMU-like samples, respectively. All the samples give a linear expression of $\varepsilon_{Hf}=1.72\varepsilon_{Nd}-2.83$.

Fig. 3 Diagram of correlations between Hf isotopic data in this study and the abundances of major and trace elements. Major and trace elements are from Niu and Batiza (1997).

Fig. 4 Correlations of Hf isotopes with Sr-Nd-Pb isotopes and with ratios of incompatible elements for near-EPR seamount lavas. The correlations are best interpreted as resulting from melting-induced mixing of a two-component mantle with the enriched component dispersed as physically distinct domains in the more depleted matrix. The correlations also indicate that both the enriched component and the depleted matrix are ancient and have

757 developed their isotopic signatures independently. The Sr-Nd-Pb isotope data are from Niu
758 et al. (2002) and the trace-elements are from Niu and Batiza (1997). Data for ridge axis
759 MORB from EPR 5-15°N are from Sims et al. (2002), Salters et al. (2011), and Gale et al.
760 (2013).
761
762 Fig. 5 Variation of (a) Yb/Nd with La/Nd and (b) La/Yb with Sm/Yb for lavas from
763 seamounts flanking the East Pacific Rise (EPR) between 5° and 15°N. Curves show range
764 in pooled melt compositions produced by variable degrees of fractional melting of a two-
765 component mantle source consisting of 10% enriched component and 90% depleted matrix,
766 calculated using the method of Stracke and Bourdon (2009). The mass fractions of enriched
767 endmembers are labelled. The enriched component is assumed to have a lower solidus
768 temperature and therefore contributes more to melting at low melt fractions, compared to
769 the more refractory matrix, which begins melting at a slightly lower pressure. Thus, unlike
770 two-component mixing of melts or sources that result in linear arrays on these diagrams,
771 the resulting melt evolution paths are curved because with increasing degree of melting,
772 the contribution to the pooled melt from the more fertile component progressively
773 decreases, which reproduce the data array defined by lavas from seamounts in this study.
774 Detailed parameters used in modeling are given in Appendix 1. Data for northern EPR
775 axial MORBs are from Salters et al. (2011), Donnelly (2002), Chauvel and Blichert-Toft
776 (2001) and references therein. “Pyroxenite” endmember better fits the seamount data.
777
778 Fig. 6 Variation of (a) La/Sm vs. $^{143}Nd/^{144}Nd$ and (b) Nb/Zr vs. $^{87}Sr/^{86}Sr$ for lavas from
779 seamounts flanking the East Pacific Rise (EPR) between 5° and 15°N. The symbols are the

780 same as in Fig. 5. The different trends reflect mixtures of melts from peridotite matrix and
781 enriched component with different solidus temperatures. Peridotite melting is assumed to
782 start at about 2.5 GPa in the spinel stability field. The dashed lines and solid lines represent
783 the onset of enriched component melting from depths significantly deeper (i.e., great
784 difference in solidus temperature between the two components) and depths similar to the
785 onset of peridotite melting (i.e., small difference in solidus temperature), respectively. The
786 compositions of depleted mantle is from Workman and Hart (2005). The pyroxenite
787 represents a 2 Ga old recycled MORB that has undergone chemical modification during
788 subduction and is isotopically similar to FOZO (Stracke and Bourdon, 2009). The isotopic
789 composition of EM1 and EM2 is from Ito and Mahoney (2005). The large variation in
790 La/Sm and Nb/Zr ratios and their good correlations with isotopes indicating a small
791 difference in solidus temperature between the two components. "EM1" endmember seems
792 to be better reproduce the array.
793
794 Fig. 7 Isotope ratios of lavas from seamounts flanking the East Pacific Rise (EPR) between
795 5° and 15°N. The initial depleted:enriched component ratio Is assumed to be 90:10. Large
796 open circles show assumed isotope ratios of each component. The dashed curves in figure
797 (b) and (c) using a mixture of 0.06:0.04 EM1:pyroxenite as the enriched component.
798 Px=pyroxenite, ϕ_m= initial proportion of EM1/EM2, and initial proportion of
799 pyroxenite=0.1- ϕ_m. Data for ridge axis MORB from EPR 5-15°N are from Sims et al.
800 (2002), Salters et al. (2011), and Gale et al. (2013). The EM1 and/or pyroxenite as the
801 enriched component can reproduce the seamount arrays.
802

803 Fig. 8 (a) ε_{Hf} versus ε_{Nd} and (b) $\Delta\varepsilon_{Hf}$ versus ε_{Nd} diagram of global MORBs. In general,
804 Atlantic MORBs and Pacific MORBs have the highest and the lowest ε_{Hf} value at given
805 Nd isotopes, respectively, and Indian MORBs lies between them. In order to show more
806 clearly, the average values are also plotted. The mantle array is $\varepsilon_{Hf}=1.59\varepsilon_{Nd}+1.28$ (Chauvel
807 et al., 2008). The published data is from Agranier et al. (2005), Blichert-Toft et al. (2005),
808 Chauvel and Blichert-Toft (2001) and refs therein, Debaille et al. (2006), Dosso et al.
809 (1993), Douglass and Schilling (1999), Fontignie and Schilling (1996), Graham et al.
810 (2006), Hamelin et al. (2011), Hanan et al. (2004), Janney et al. (2005), Kempton et al.
811 (2000, 2002), Klein et al. (1988), Mahoney et al. (2002), Meyzen et al. (2007), Nowell et
812 al. (1998), Patchett (1983), Patchett and Tatsumoto (1980), Pyle et al. (1992), Salters
813 (1996), Salters and White (1998), Salters et al. (2011) and refs therein, Schilling et al. (1994,
814 1999, 2003), Sims et al. (2002), Yu et al. (1997). The difference in $\Delta\varepsilon_{Hf}$ values between
815 Pacific, Atlantic and Indian MORBs is likely result from various contribution of residual
816 continental lithospheric mantle with high $\Delta\varepsilon_{Hf}$ values. Data for SCLM are from Bianchini
817 et al. (2007), Carlson et al. (2004), Chu et al. (2009), Lapen et al. (2005), Schmidberger et
818 al. (2002), Simon et al. (2007), and Witting et al. (2007).
819
820 Fig. 9 The correlations between parent-daughter and isotopes ratios for Rb-Sr, Sm-Nd and
821 Lu-Hf give pseudochron ages of 182±33 Ma, 276±50 Ma and 387±93Ma, respectively.
822 These different “ages” have no age significance, but are best explained as resulting from
823 melting-induced mixing with the pseudochron slopes controlled by the compositions of the
824 enriched component and the depleted end-member. The two end-members have
825 independently developed their distinct chemical and isotopic signatures. The symbols are

826 the same as in Fig. 4. The fractional melting modeling can reproduce the arrays. The trace-
827 element and Sr-Nd isotope compositions are from Niu and Batiza (1997) and Niu et al.
828 (2002). Data for ridge axis MORB from EPR 5-15°N are from Sims et al. (2002), Salters
829 et al. (2011), and Gale et al. (2013).
830
831 Fig. A1 The locations of EPR 5-15°N and Garrett Transform in the Pacific (According to
832 Amante and Eakins, 2009).

Table 1 Hf isotopic data of glass samples from near-ridge seamounts between 5 and 15°N EPR

Sample	Type	Latitude/°N	Longitude/°W	Depth/m	$^{176}Hf/^{177}Hf$	2σ	ε_{Hf}
R74-5	**N**	10.62	103.84	2320.00	0.283174	± 0.000012	14.22
R7-13	**N**	8.14	103.19	2020.00	0.283189	± 0.000015	14.76
R3-4	**E**	5.78	102.21	1773.00	0.283212	± 0.000013	15.56
R3-1	**N**	5.78	102.21	1773.00	0.283194	± 0.000014	14.93
R3-3	**N**	5.78	102.21	1773.00	0.283201	± 0.000017	15.18
R1-14	**N**	5.77	102.18	1834.00	0.283187	± 0.000012	14.66
R66-1	**N**	10.14	103.34	2600.00	0.283189	± 0.000013	14.75
R28-8	**N**	8.81	103.90	1984.00	0.283156	± 0.000010	13.57
R103-13	**N**	13.84	103.80	2870.00	0.283201	± 0.000010	15.16
R22-1	**N**	8.90	104.10	2749.00	0.283161	± 0.000011	13.77
R25-1	**N**	8.88	103.79	1980.00	0.283158	± 0.000013	13.64
R65-1	**N**	10.13	103.41	2074.00	0.283186	± 0.000013	14.63
R8-8	**N**	8.34	103.06	3180.00	0.283153	± 0.000013	13.49
R19-4	**N**	8.94	104.41	2267.00	0.283158	± 0.000013	13.65
R60-1	**N**	10.00	104.91	2640.00	0.283213	± 0.000014	15.61
R71-2	**N**	10.26	103.74	3380.00	0.283173	± 0.000006	14.18
R21-6	**E**	8.89	104.14	2657.00	0.283152	± 0.000011	13.46
R16-2	**N**	8.84	104.57	2985.00	0.283155	± 0.000013	13.56
R62-4	**E**	10.03	104.19	2320.00	0.283167	± 0.000015	13.95
R24-3	**N**	8.97	103.87	3054.00	0.283142	± 0.000008	13.10
R102-1	**E**	13.22	102.68	2350.00	0.283178	± 0.000013	14.37
R96-24	**E**	13.07	103.45	2577.00	0.283209	± 0.000011	15.46
R72-2	**E**	10.38	103.93	2748.00	0.283120	± 0.000010	12.29
R4-2	**E**	5.60	103.02	2263.00	0.283110	± 0.000009	11.94
R73-1	**E**	10.38	103.92	2547.00	0.283124	± 0.000010	12.43
R32-1	**E**	9.09	104.92	3025.00	0.283084	± 0.000012	11.03
R110-4	**E**	14.14	104.36	2760.00	0.283136	± 0.000009	12.86
R18-3	**E**	8.93	104.46	2720.00	0.283061	± 0.000011	10.21
R80-6	**E**	11.80	103.25	1619.00	0.283144	± 0.000008	13.14
R17-1&2	**E**	8.91	104.57	2715.00	0.283027	± 0.000007	9.01
R109-5	**E**	14.15	104.30	2610.00	0.283110	± 0.000011	11.96
R83-2	**E**	11.24	103.59	2900.00	0.283084	± 0.000008	11.04
R79-2	**E**	11.79	103.25	1620.00	0.283047	± 0.000011	9.72
R78-5	**E**	11.22	103.58	2450.00	0.283043	± 0.000009	9.58
R13-1	**Alkali**	8.40	104.07	2140.00	0.282974	± 0.000007	7.15
R15-1	**Alkali**	8.76	104.54	1682.00	0.282966	± 0.000008	6.86

Fig. 1

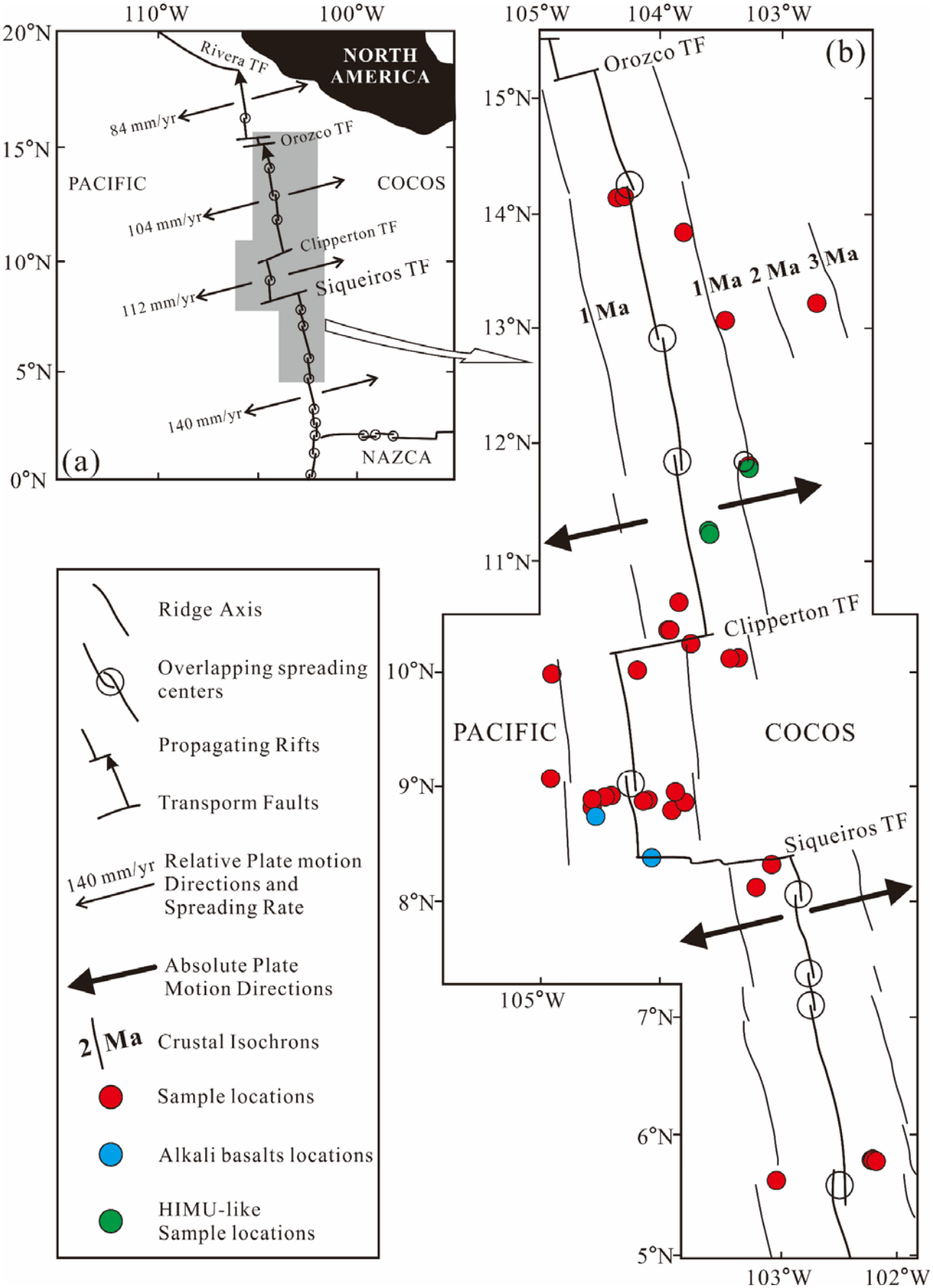
110°W
100°W
20°N
15°N
10°N
5°N
0°N
NORTH AMERICA
Rivera TF
84 mm/yr
Orozco TF
PACIFIC
COCOS
104 mm/yr
Clipperton TF
Siqueiros TF
112 mm/yr
140 mm/yr
NAZCA
(a)
105°W
104°W
103°W
(b)
Orozco TF
15°N
14°N
13°N
12°N
11°N
10°N
9°N
8°N
7°N
6°N
5°N
105°W
103°W
102°W
1 Ma
1 Ma 2 Ma 3 Ma
Clipperton TF
PACIFIC
COCOS
Siqueiros TF
Ridge Axis
Overlapping spreading centers
Propagating Rifts
Transporm Faults
140 mm/yr
Relative Plate motion Directions and Spreading Rate
Absolute Plate Motion Directions
2 Ma
Crustal Isochrons
Sample locations
Alkali basalts locations
HIMU-like Sample locations

Fig. 2

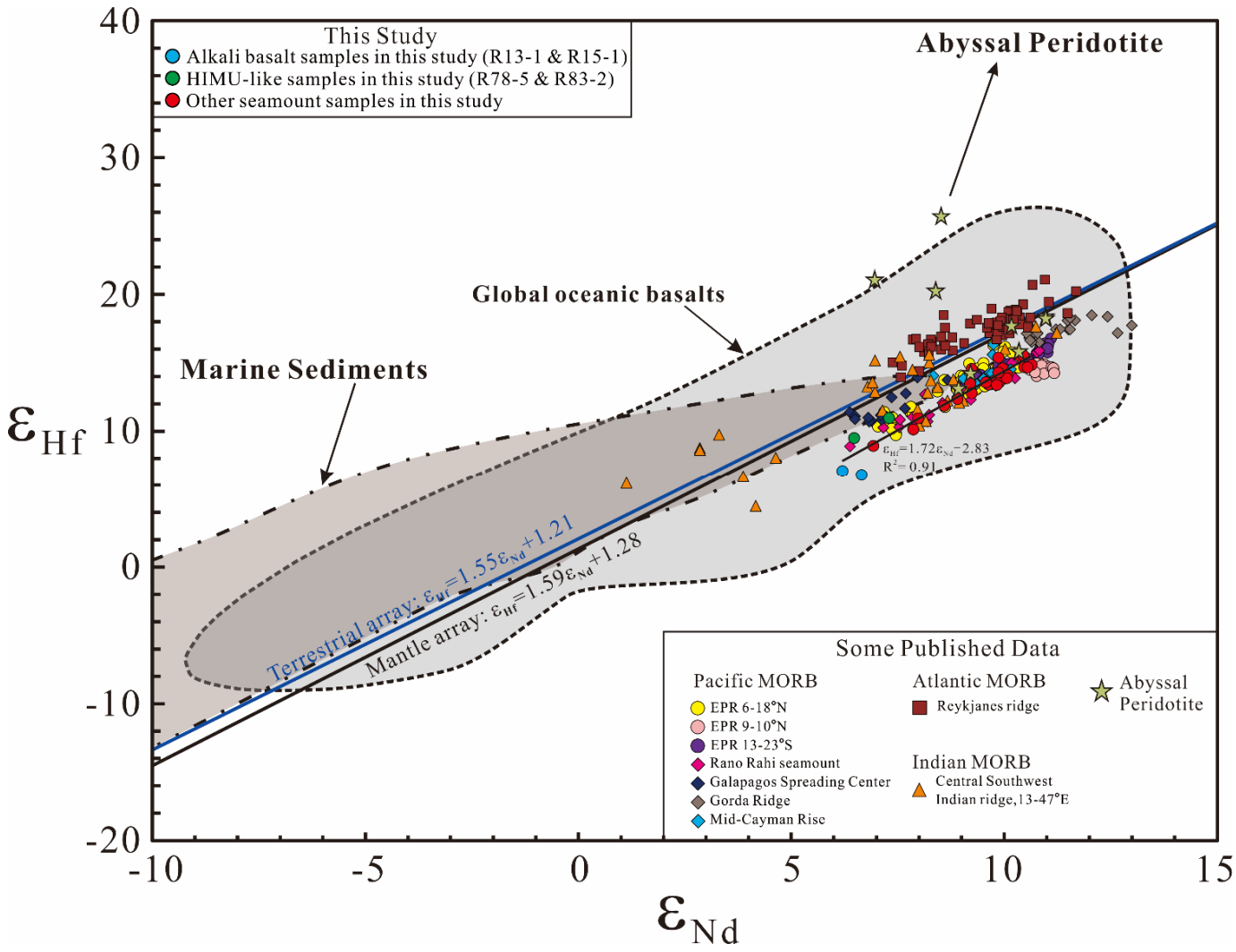
This Study
Alkali basalt samples in this study (R13-1 & R15-1)
HIMU-like samples in this study (R78-5 & R83-2)
Other seamount samples in this study
Abyssal Peridotite
Global oceanic basalts
Marine Sediments
Terrestrial array: εHf=1.55εNd+1.21
Mantle array: εHf=1.59εNd+1.28
εHf=1.72εNd−2.83
R2= 0.91
Some Published Data
Pacific MORB
EPR 6-18°N
EPR 9-10°N
EPR 13-23°S
Rano Rahi seamount
Galapagos Spreading Center
Gorda Ridge
Mid-Cayman Rise
Atlantic MORB
Reykjanes ridge
Indian MORB
Central Southwest Indian ridge,13-47°E
Abyssal Peridotite
εHf
εNd
40
30
20
10
0
-10
-20
-10
-5
0
5
10
15

Fig. 3

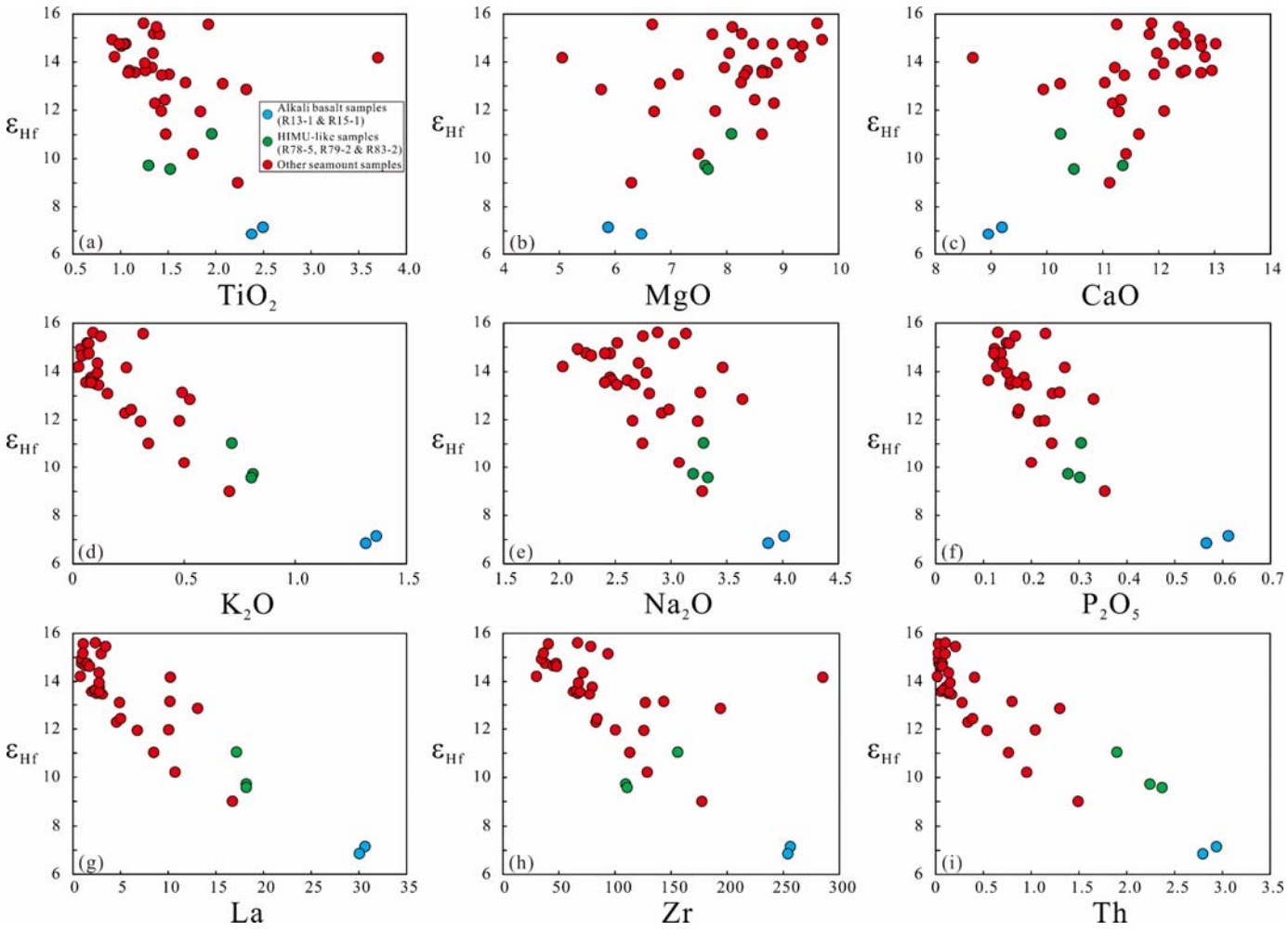
Alkali basalt samples (R13-1 & R15-1)
HIMU-like samples (R78-5, R79-2 & R83-2)
Other seamount samples
(a)
(b)
(c)
(d)
(e)
(f)
(g)
(h)
(i)
εHf
TiO2
MgO
CaO
K2O
Na2O
P2O5
La
Zr
Th

Fig. 4

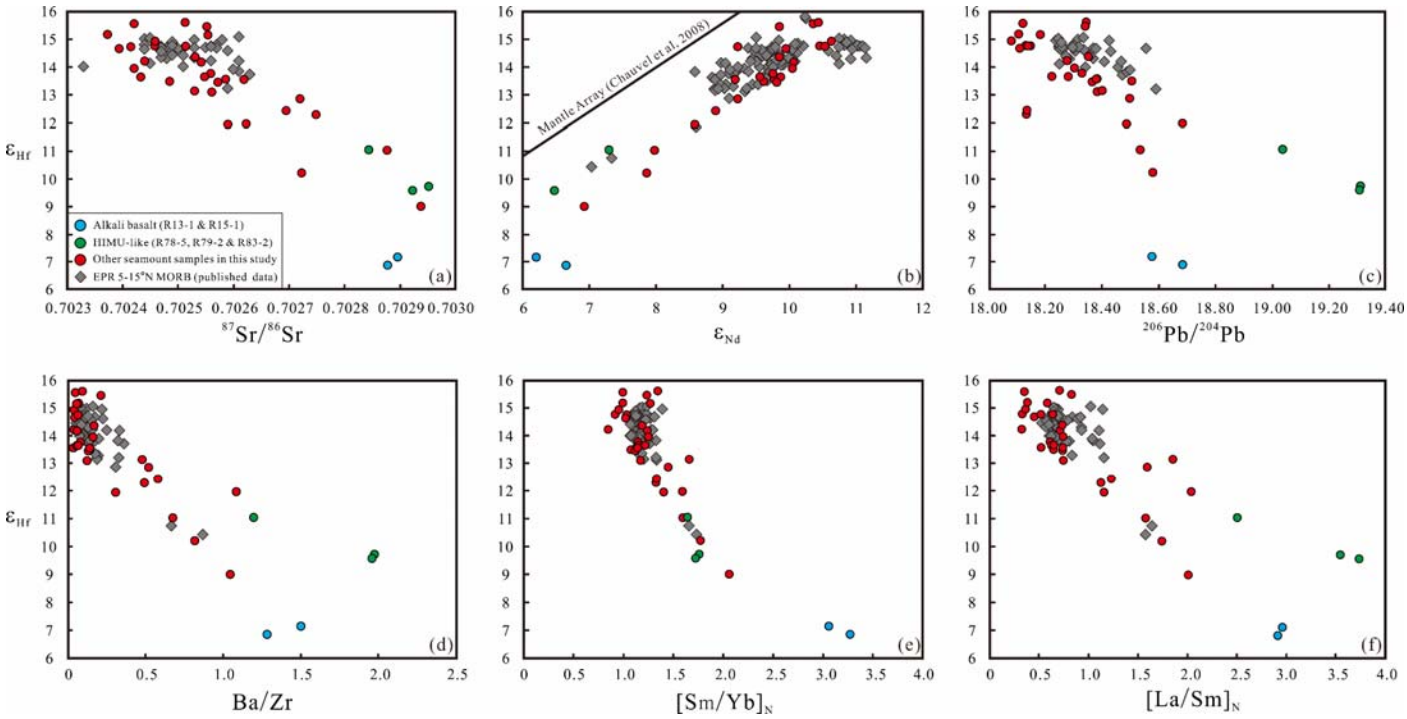
Alkali basalt (R13-1 & R15-1)
HIMU-like (R78-5, R79-2 & R83-2)
Other seamount samples in this study
EPR 5-15°N MORB (published data)
Mantle Array (Chauvel et al., 2008)
(a)
(b)
(c)
(d)
(e)
(f)
εHf
εNd
87Sr/86Sr
206Pb/204Pb
Ba/Zr
[Sm/Yb]N
[La/Sm]N

Fig. 5

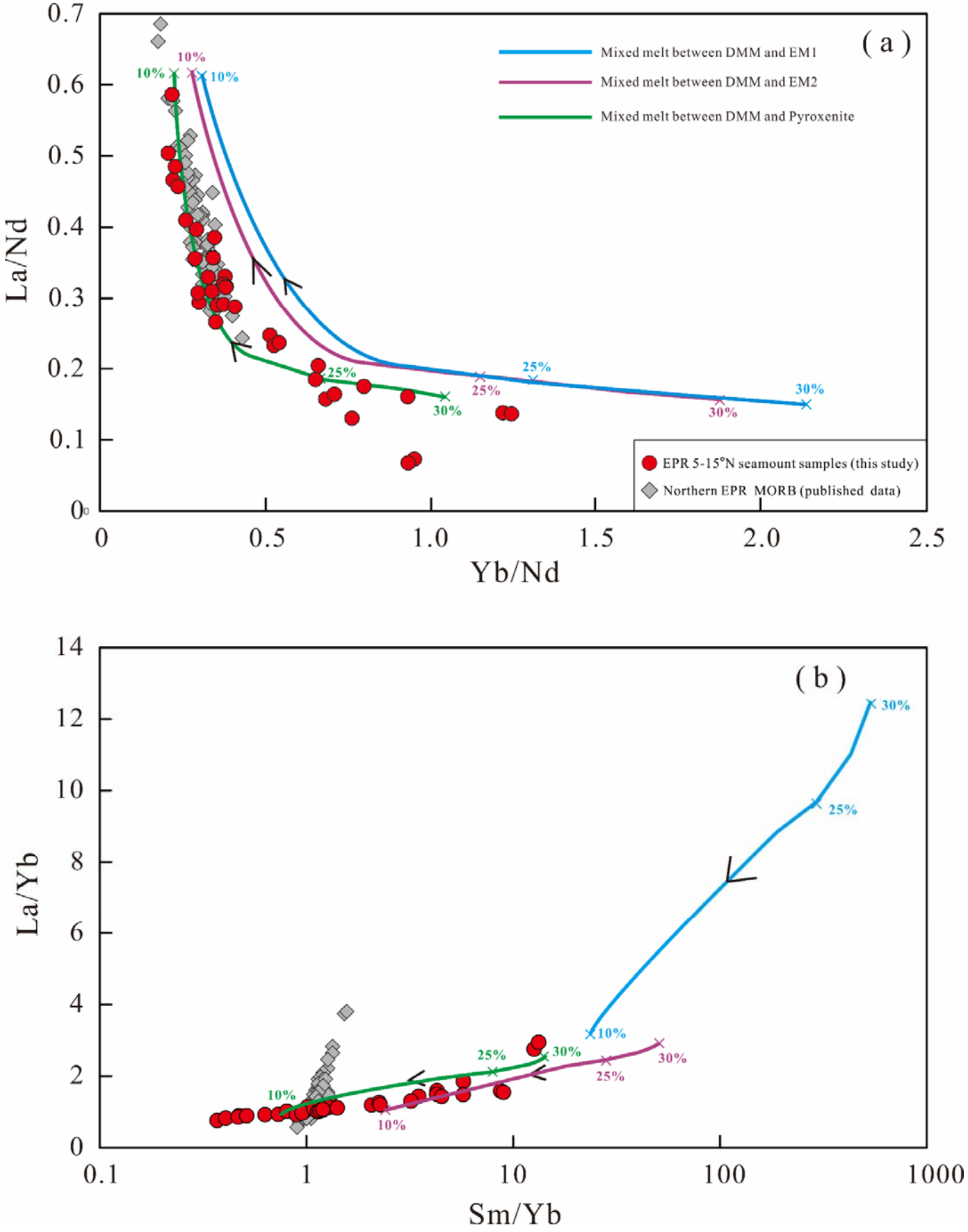
(a)
Mixed melt between DMM and EM1
Mixed melt between DMM and EM2
Mixed melt between DMM and Pyroxenite
EPR 5-15°N seamount samples (this study)
Northern EPR MORB (published data)
La/Nd
Yb/Nd
0.7
0.6
0.5
0.4
0.3
0.2
0.1
0
0.5
1.0
1.5
2.0
2.5
10%
25%
30%
(b)
La/Yb
Sm/Yb
14
12
10
8
6
4
2
0
0.1
1
10
100
1000

Fig. 6

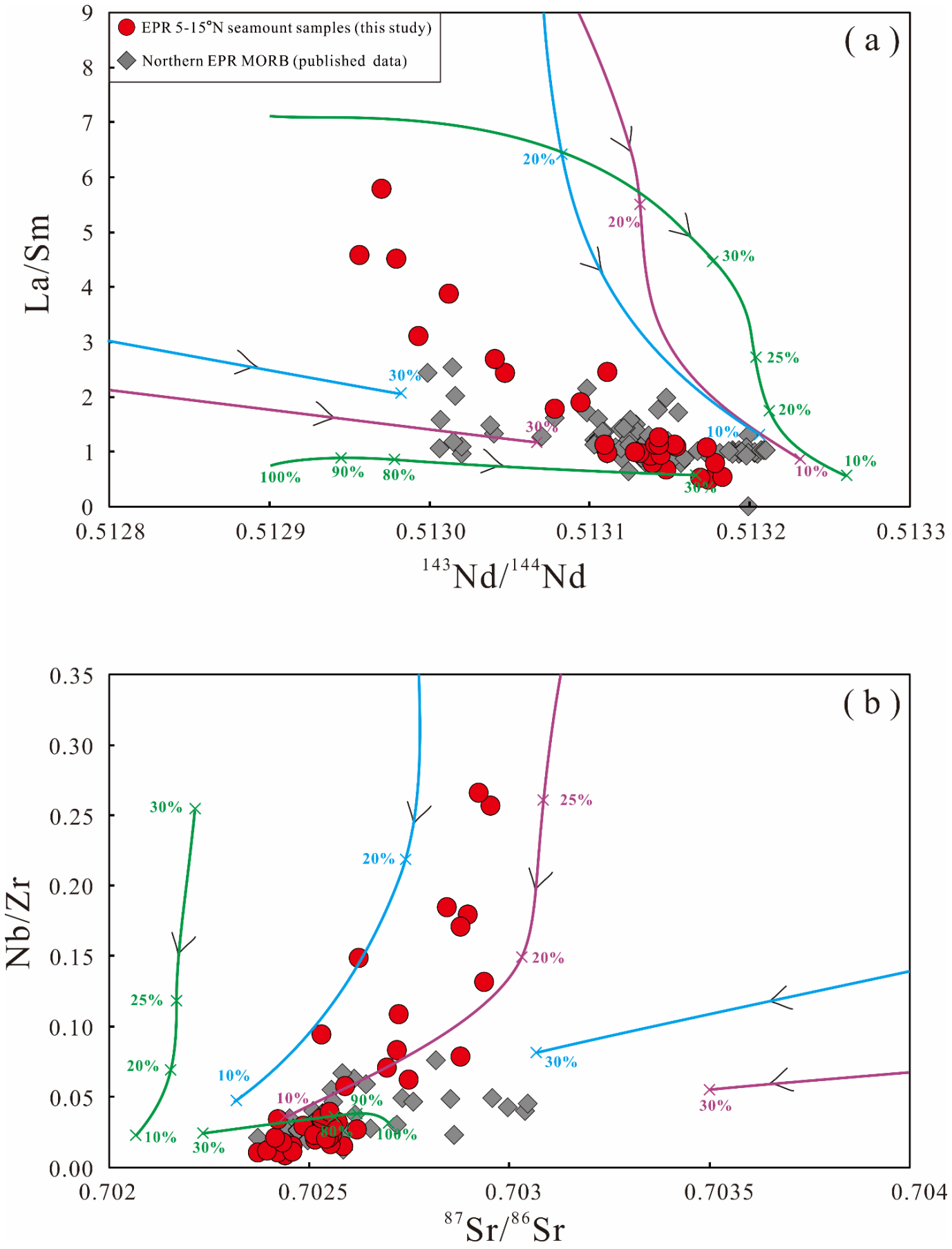
EPR 5-15°N seamount samples (this study)
Northern EPR MORB (published data)
(a)
La/Sm
143Nd/144Nd
0.5128
0.5129
0.5130
0.5131
0.5132
0.5133
0
1
2
3
4
5
6
7
8
9
20%
30%
25%
10%
100%
90%
80%
(b)
Nb/Zr
87Sr/86Sr
0.702
0.7025
0.703
0.7035
0.704
0.00
0.05
0.10
0.15
0.20
0.25
0.30
0.35

Fig. 7

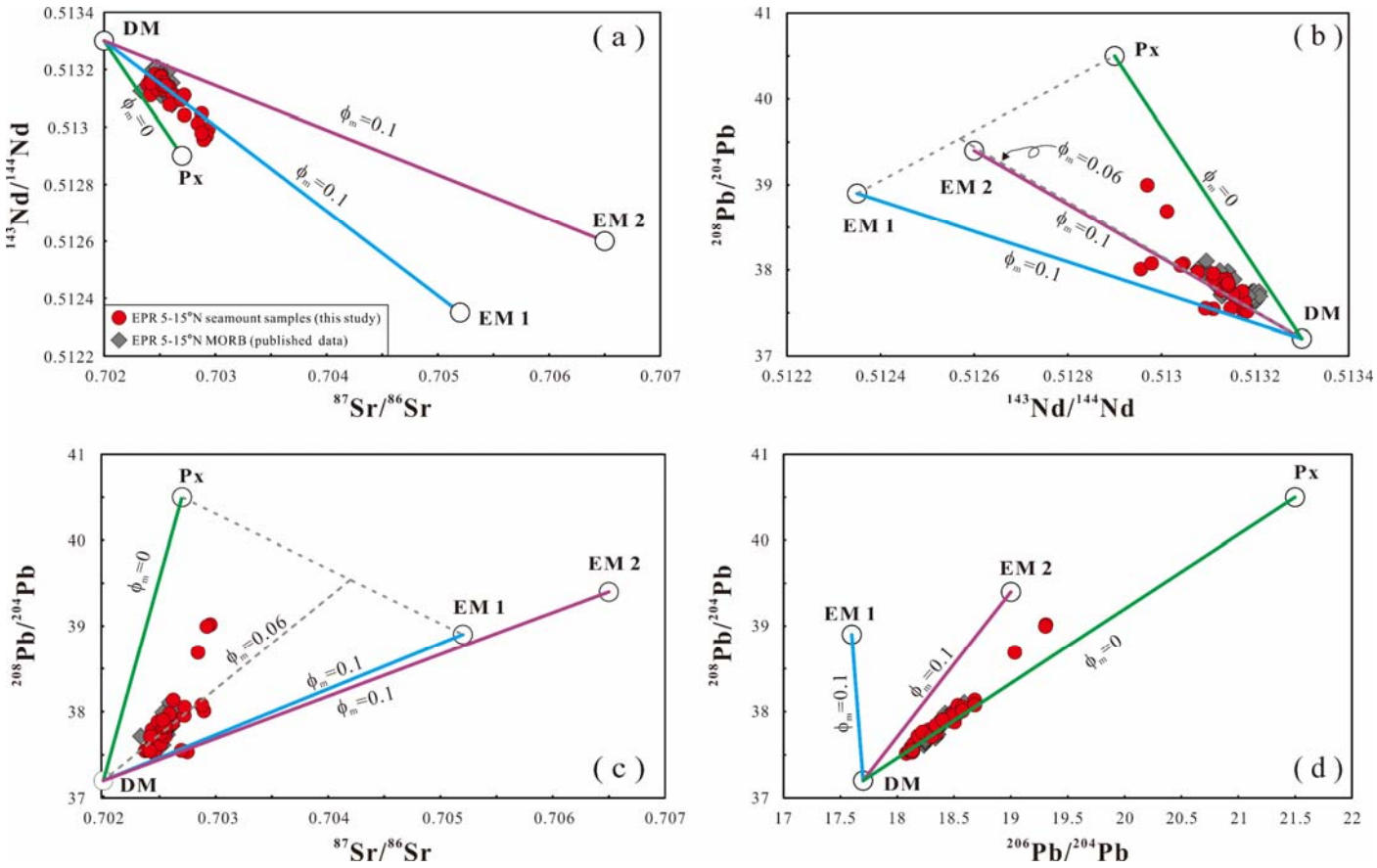
(a)
DM
Px
EM 2
EM 1
ϕ_m=0
ϕ_m=0.1
ϕ_m=0.1
EPR 5-15°N seamount samples (this study)
EPR 5-15°N MORB (published data)
$^{143}Nd/^{144}Nd$
$^{87}Sr/^{86}Sr$
(b)
Px
EM 2
EM 1
DM
ϕ_m=0.06
ϕ_m=0
ϕ_m=0.1
ϕ_m=0.1
$^{208}Pb/^{204}Pb$
$^{143}Nd/^{144}Nd$
(c)
Px
EM 2
EM 1
DM
ϕ_m=0
ϕ_m=0.06
ϕ_m=0.1
ϕ_m=0.1
$^{208}Pb/^{204}Pb$
$^{87}Sr/^{86}Sr$
(d)
Px
EM 2
EM 1
DM
ϕ_m=0.1
ϕ_m=0.1
ϕ_m=0
$^{208}Pb/^{204}Pb$
$^{206}Pb/^{204}Pb$

Fig. 8

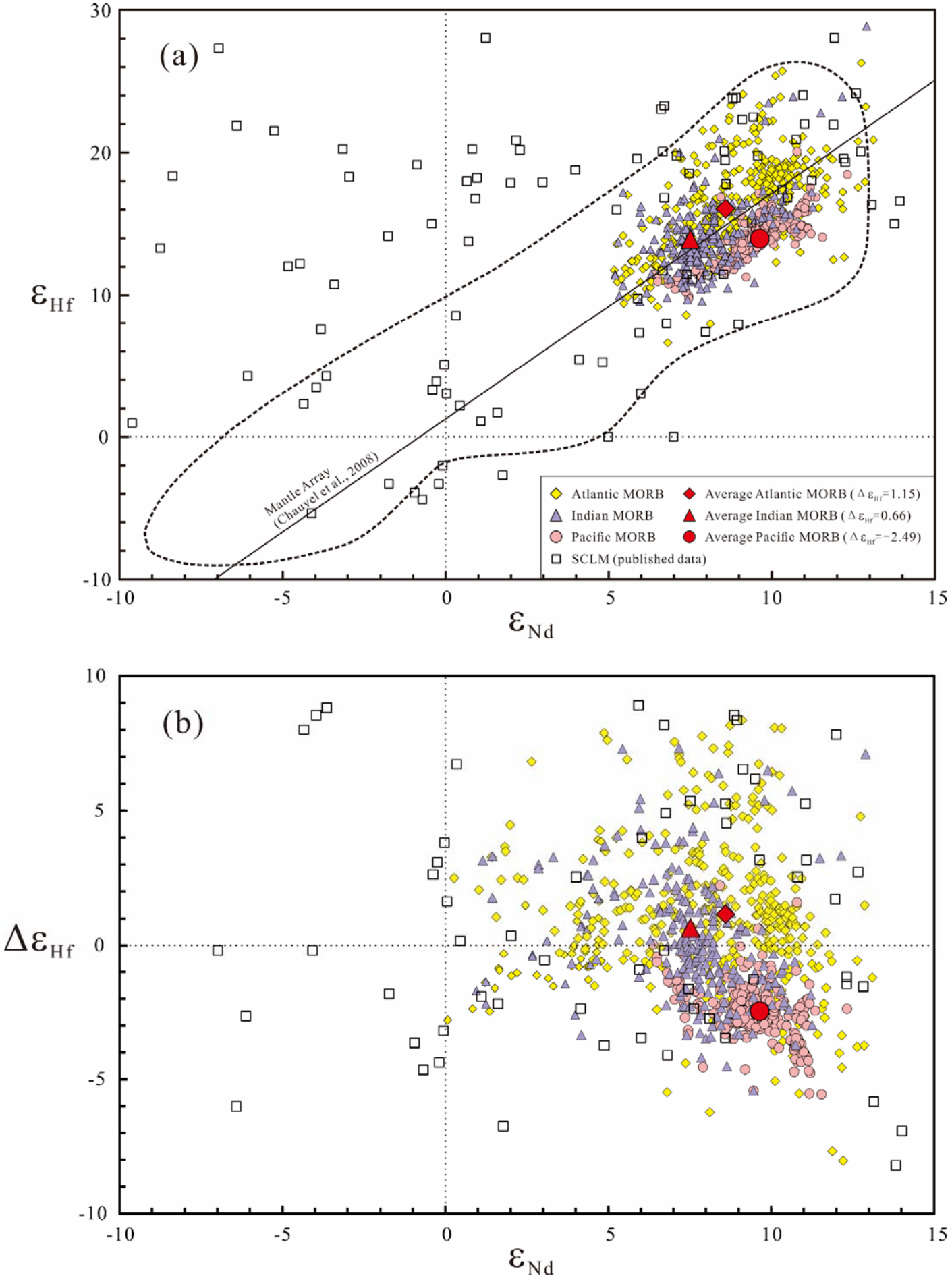
(a)
30
20
10
0
-10
ε_{Hf}
-10
-5
0
5
10
15
ε_{Nd}
Mantle Array
(Chauvel et al., 2008)
Atlantic MORB
Indian MORB
Pacific MORB
SCLM (published data)
Average Atlantic MORB ($\Delta\varepsilon_{Hf}$=1.15)
Average Indian MORB ($\Delta\varepsilon_{Hf}$=0.66)
Average Pacific MORB ($\Delta\varepsilon_{Hf}$=−2.49)
(b)
10
5
0
-5
-10
$\Delta\varepsilon_{Hf}$
-10
-5
0
5
10
15
ε_{Nd}

Fig. 9

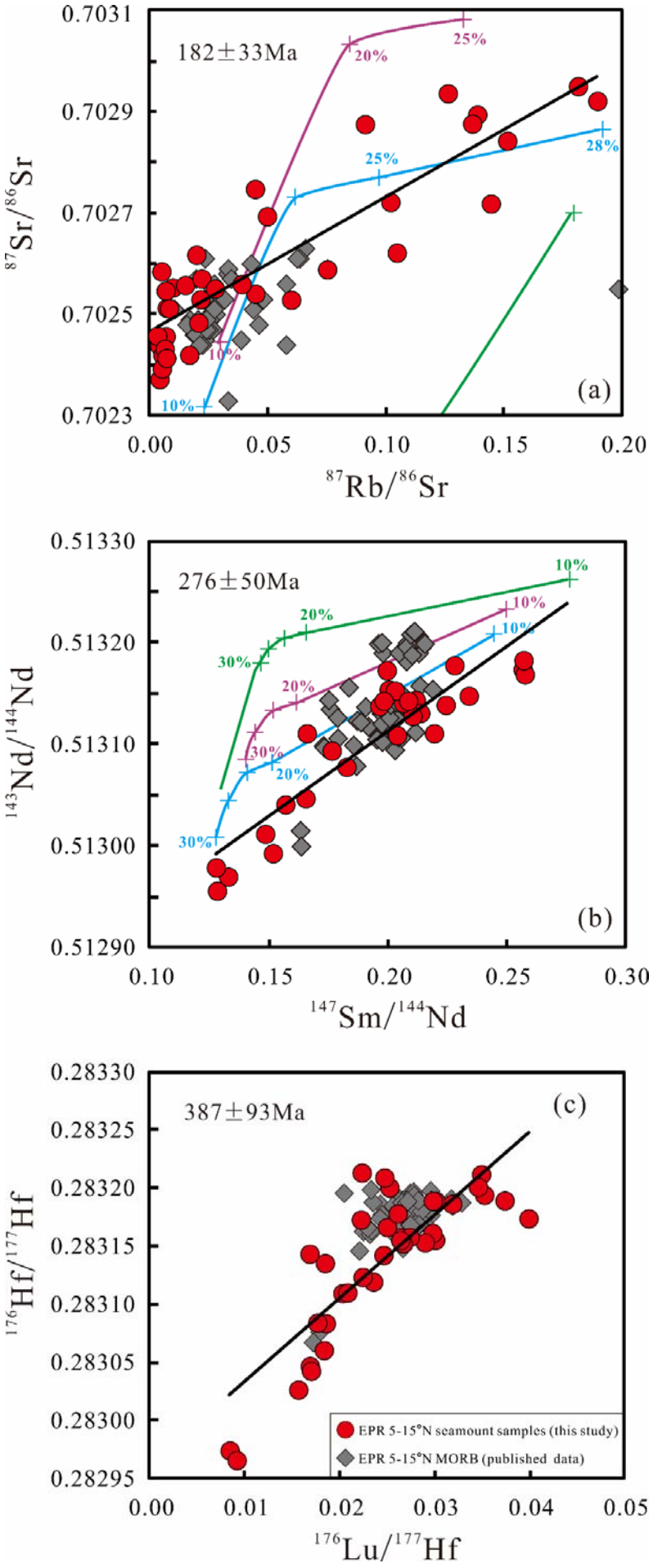
182±33Ma
25%
20%
28%
25%
10%
10%
(a)
0.7031
0.7029
0.7027
0.7025
0.7023
0.00
0.05
0.10
0.15
0.20
87Sr/86Sr
87Rb/86Sr
276±50Ma
10%
20%
10%
30%
20%
10%
30%
20%
30%
(b)
0.51330
0.51320
0.51310
0.51300
0.51290
0.10
0.15
0.20
0.25
0.30
143Nd/144Nd
147Sm/144Nd
387±93Ma
(c)
0.28330
0.28325
0.28320
0.28315
0.28310
0.28305
0.28300
0.28295
0.00
0.01
0.02
0.03
0.04
0.05
176Hf/177Hf
176Lu/177Hf
EPR 5-15°N seamount samples (this study)
EPR 5-15°N MORB (published data)

Fig. A1